POLITECNICO DI TORINO

Master's Degree in Energy and Nuclear Engineering 2024/2025

Dynamic Behaviour and Hydrogen Crossover Modelling in PEM Water Electrolyzers

Author: Maria Chiara Scarafia

Supervisor: Marta Gandiglio, Eduardo Prieto-Araujo

Cosupervisor: Paolo Marocco, Lorenzo Bruno

Esteban Gonzalez Iakl, Massimo Santarelli





CONTENTS page 3

Contents

Al	ostra		5
1	Intr	duction and Objectives	7
	1.1	Economical and Political background	7
	1.2	Types of Hydrogen	9
		1.2.1 Black or brown hydrogen	9
		1.2.2 Grey hydrogen	9
			10
			10
			11
			11
			11
			12
	1.3		12
_			
2		0	15 15
	2.1	· · · · · · · · · · · · · · · · · · ·	15
	2.2		18
		· · · · · · · · · · · · · · · · · · ·	18
			19
			20
		2.2.4 Proton Exchange Membrane (PEM) water electrolyser	20
3	Che	nical degradation of a PEMWE	23
	3.1		23
		3.1.1 Electrocatalyst and catalyst layer degradation	23
			24
			25
		3.1.4 Current collectors degradation	25
4	Mat	ematical model	27
	4.1		- <i>-</i> 27
	4.2		<u> </u>
	4.3		31
	4.4		32
	4.5		35
_	ъ.		•
5			39 39
	5.1		
	5.2 F. 2		41
	5.3		44 45
		1	
		1 1	50 54
		5.3.3 PV input power	54
6	Part		61
	6.1	Degradation consequence: Hydrogen and Oxygen crossover	61

page 4 Master Thesis

7	Con	aclusion	67
8	Sim	ulink model blocks	69
	8.1	Anode	69
	8.2	Cathode	70
	8.3	Membrane	70
	8.4	Voltage	72
	8.5	Thermal Block	73
Bi	bliog	graphy	77
Li	st of	Figures	79
Li	st of	Tables	82
A	knov	wledgments	85

CONTENTS page 5

Abstract

The goal of this thesis is the development of a realistic dynamic model of a Proton Exchange Membrane (PEM) electrolyser with respect to the already existing models present in the literature.

Initially, a base model was constructed using standard equations to describe the typical operating behavior of an electrolyzer. Implementations have been done to enhance the model realism and to implement the common models of the literature.

A differentiation between the liquid and vapor phases of water within the electrodes has been introduced through a formulation based on partial pressures. In addition, the development of the internal double layer at the anode and cathode has been modeled in order to reproduce a more realistic behavior during the transient and a time delay response with respect to a dynamic changing input current.

In the end, the phenomenon of hydrogen crossover from cathode to anode was introduced to assess the safety conditions during the electrolyzer performance under different operating current densities and temperatures, monitoring the satisfaction of the industrial safety limit.

The behavior of the electrolyser has been studied considering initially two ideal cases, with a constant input current and a step current behavior, and secondly the power produced by a photovoltaic plant.

The model was simulated in the Matlab/Simulink® environment.

1 Introduction and Objectives

1.1 Economical and Political background

Over the past decades, global warming has become rapidly one of the most important problems humanity has to face. The consequences due to the constant rising of the temperatures, to the fast changing climate conditions across different regions in the world, to small changes in natural habitats and the risk on human health are becoming more and more intense and relevant.

The main cause of CO_2 emissions can be attributed to the use of fossil fuels.

The industrial sector typically accounts for the largest share of emissions, including oil and gas production as well as the manufacturing of materials and chemicals. The energy sector generally follows the industrial one in the second position.

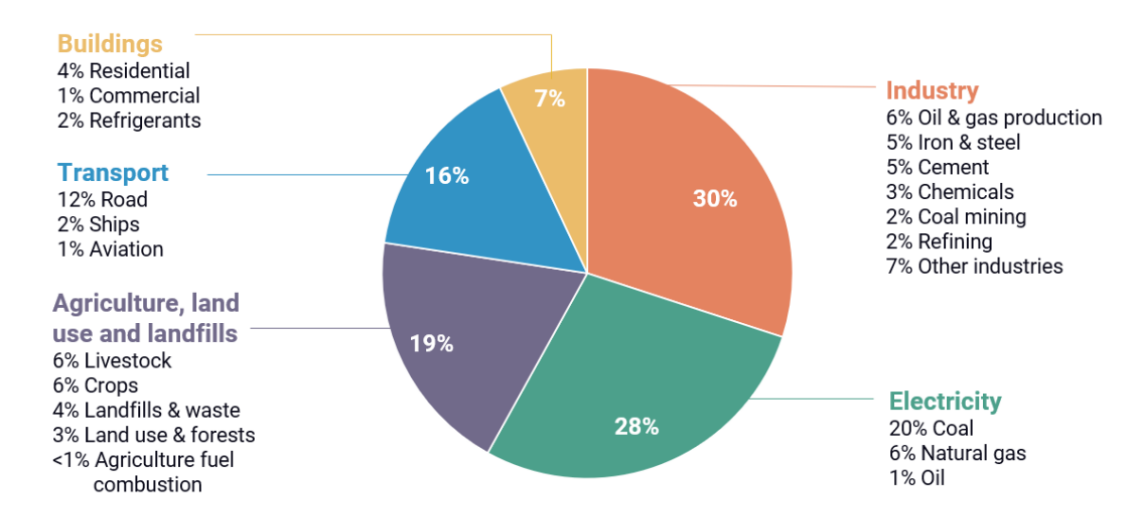


Figure 1: Sectors contributions to GHG emissions in 2022 [1]

From 1990 to 2023, greenhouse gas emissions in the European Union decreased by 37%, from 4.635 to 2.908 million tonnes of CO_2 equivalent (MtCO₂eq), a remarkable outcome due to the optimization of technologies and procedures and, regarding the last years, the new environmental policies.

In 2023 on a global level coal accounted for 41% of global CO_2 emissions, followed by oil at 32%, natural gas at 23%, and cement production at 4%[2][3].

Various proposals and solutions have been formulated during the past years to find a common path towards climate safeguard and emissions reduction, especially through economic and social transformations. The Paris Agreement, in 2015, was signed by 196 Parties during COP21 with the primary goal of "keeping the increase in global average temperature below 2 $^{\circ}$ C above pre-industrial levels and pursuing efforts to limit it to 1.5 $^{\circ}$ C" [4].

To invest in that goal, technology development to reduce particle emissions and greenhouse gasses have been developed and updated, while renewable energies have become more and more widely spread and incentivized, along with circular economy approach and reduction-recirculation of wastes.

As an example, at the European level, the European Green Deal represents an important stone towards climate neutrality. One of its key milestones is the "Fit for 55" package of twelve pro-

page 8 Master Thesis

posals, which sets a legally binding target of reducing net greenhouse gas emissions by at least 55% by 2030 compared to 1990 levels.

The Green Deal also prioritizes:

- Promotion of a circular economy and resource efficiency in order to reduce the wastes or recirculate them in order to make a more efficient and less pollutant production especially in the industry field.
- Protection of biodiversity and ecosystems, extremely put in danger by climate changes.
- Investment in research and innovation to accelerate the energy transition.
- Wider deployment of renewable energy, including in the transport sector.

Despite the progresses achieved over the last decades, the data from 2025 clearly show that further efforts are needed to accelerate the shift away from fossil fuels. The trends show an increase of global GHG emissions during the years, even if during the last two years, plus the beginning of the current one, the curves got closer showing the effects obtained from the deployment of renewable energies.

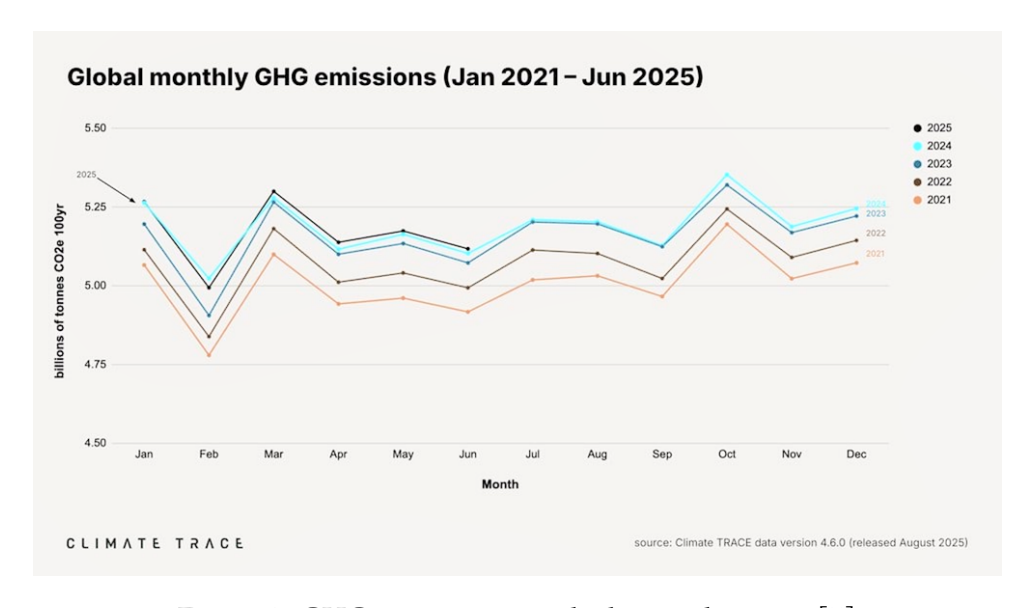


Figure 2: GHG emissions trends during the years [5]

Nevertheless, during the first months of the 2025, United States and Europe combined emissions reached 801 MtCO_2 between January and March, with an increase of 7% compared to the first months of the previous year. Instead, China, which has been one of the largest contributor in terms of pollutant emissions during the past decades due to its fast growing industrialization policies, has recorded an emission drop during this year thanks to the accelerated deployment of renewable energy. Until now, 30.99 billion tonnes of CO_2 equivalent were already produced globally, slightly above the levels recorded in the same period of 2024[6][7].

Furthermore, apart from the environmental aspects, the unstable economic and political situations dictated by direct political conflicts, by wars of economy due to the supply of resources and convenience pacts between states, regarding oil or natural gas, are leading to the increas-

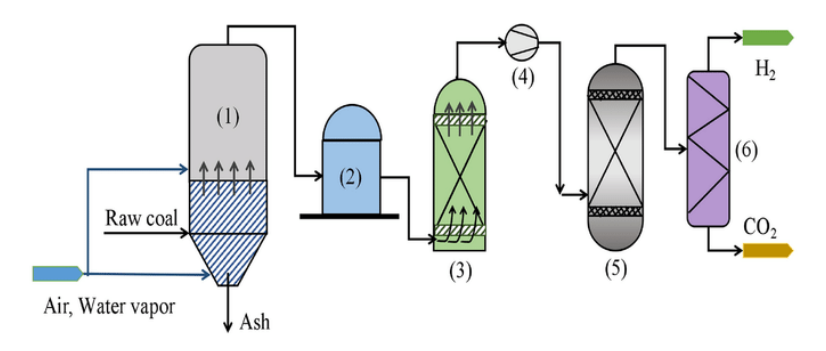
ingly urgent need to become more energetically independent from fossil fuels detained from others. Also for this reason, renewable sources have found more space in projects during the recent years. Although, apart from the traditional renewable sources such as solar, wind, and hydropower, attention has been given recently to alternative emerging solutions such as green hydrogen, energy storage technologies, and sector coupling strategies.

1.2 Types of Hydrogen

In particular, hydrogen is a versatile energy carrier that can be used in a lot of different applications. General usages involve it as an alternative fuel in new generation vehicles, as a tool to store energy through electrolysis process, and in the production of chemicals industry. Based on the technology and the processes used for its production, and on its eventual environmenal impact, a specific a color is assigned for distinction and denomination.

1.2.1 Black or brown hydrogen

This kind of hydrogen is produced through gasification of black coal or brown coal (lignite). During this process a carbon based raw material is converted into syngas using air and steam, obtaining a mixture of hydrogen and carbon monoxide and a small amount of methane and carbon dioxide. Around 20 kg of CO_2 is released for every kg of brown/black hydrogen produced [8]. This is considered to be the less friendly approach in hydrogen production.



(1) Coal gasifier, (2) Gas tank, (3) Desulfurization tower, (4) Compressor, (5) CO converter, (6)

PSA hydrogen extraction tower

Figure 3: General scheme of black H2 production through coal gasification [9]

1.2.2 Grey hydrogen

It is obtained from natural gas through steam methane reforming. The steam methane reforming process produces syngas through a reaction of hydrocarbons and steam at high pressures and temperatures. The process produces a significant amount of CO_2 emissions and it is the most common way of hydrogen production in the world (95%).

page 10 Master Thesis

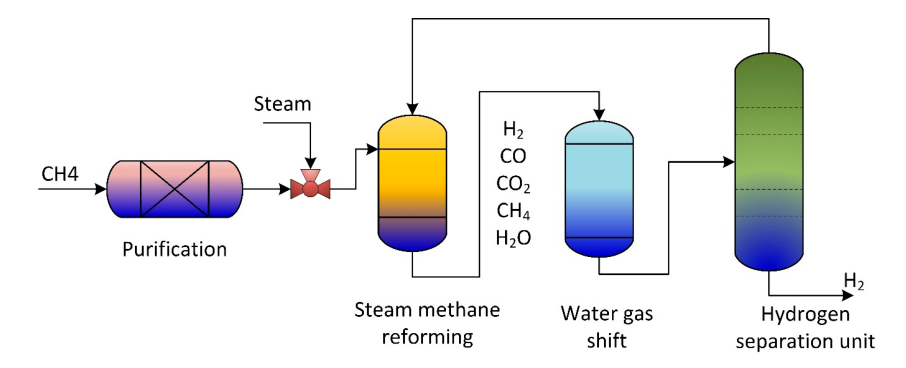


Figure 4: Steam methane reforming for grey H2 production [10]

1.2.3 Blue hydrogen

It is obtained from a fossil fuel source but it's coupled with carbon capture, utilization and storage system (CCUS) to reduce the carbon dioxide emissions. In this case the production is cleaner with respect to grey hydrogen but the cost due to CCS technology is higher.

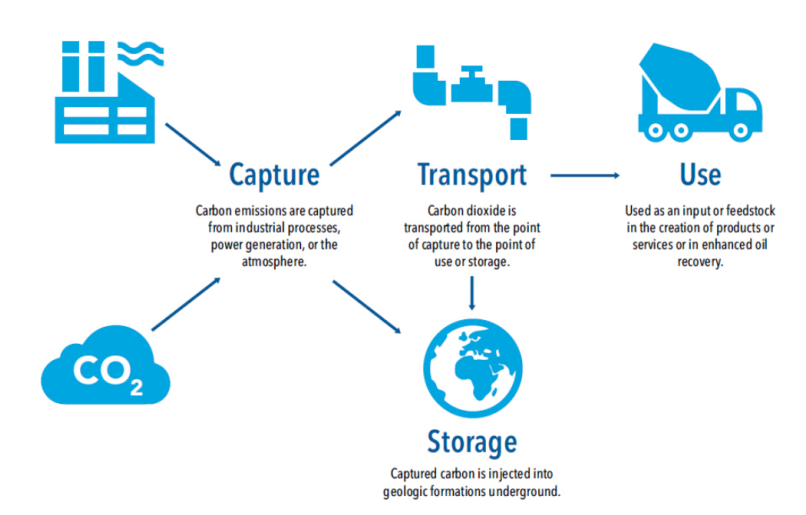


Figure 5: CCUS scheme principle [11]

1.2.4 Green or renewable hydrogen

It is produced from renewable energy sources through electrolysis process in an electrolyser. The device uses the input power to splits water molecules into hydrogen and oxygen. The power can be sent with a direct coupling with the electrolyser or through grid connection. The associated costs are significantly higher with respect to the previously mentioned options, but no CO_2 emissions are generated.



Figure 6: Green H2 production scheme [12]

1.2.5 Pink hydrogen

It is produced by water electrolysis through nuclear power. If heat is also used, it is called Purple hydrogen. It is not widely used, especially in Europe where the few cases of nuclear power are mainly used for grid electricity applications.

1.2.6 Turquoise hydrogen

It is obtained from methane pyrolysis. Natural gas is split into hydrogen and solid carbon, which can be used in further application leading to a lower cabon footprint with respect to grey hydrogen [8].

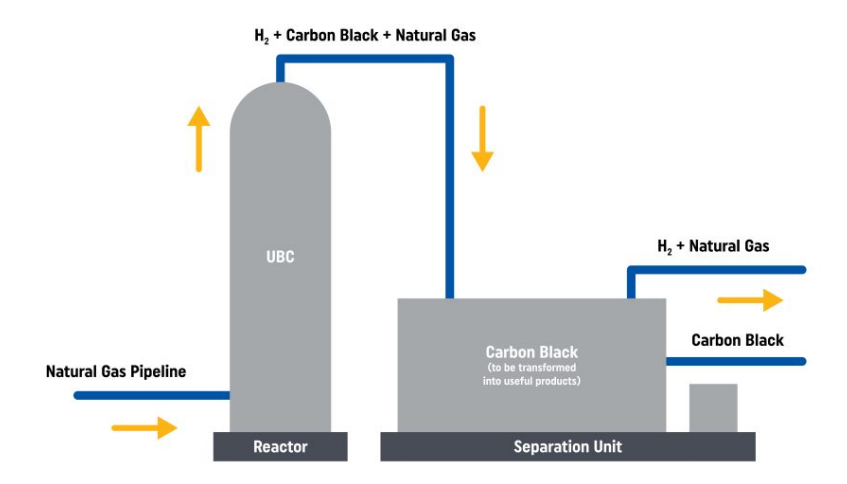


Figure 7: Methane pyrolysis for hydrogen production [13]

1.2.7 Yellow hydrogen

It is produced through electrolysis using power from the grid. The CO_2 emissions vary depending on how the power in the grid has been produced, which can come from renewable sources or fossil fuels.

page 12 Master Thesis

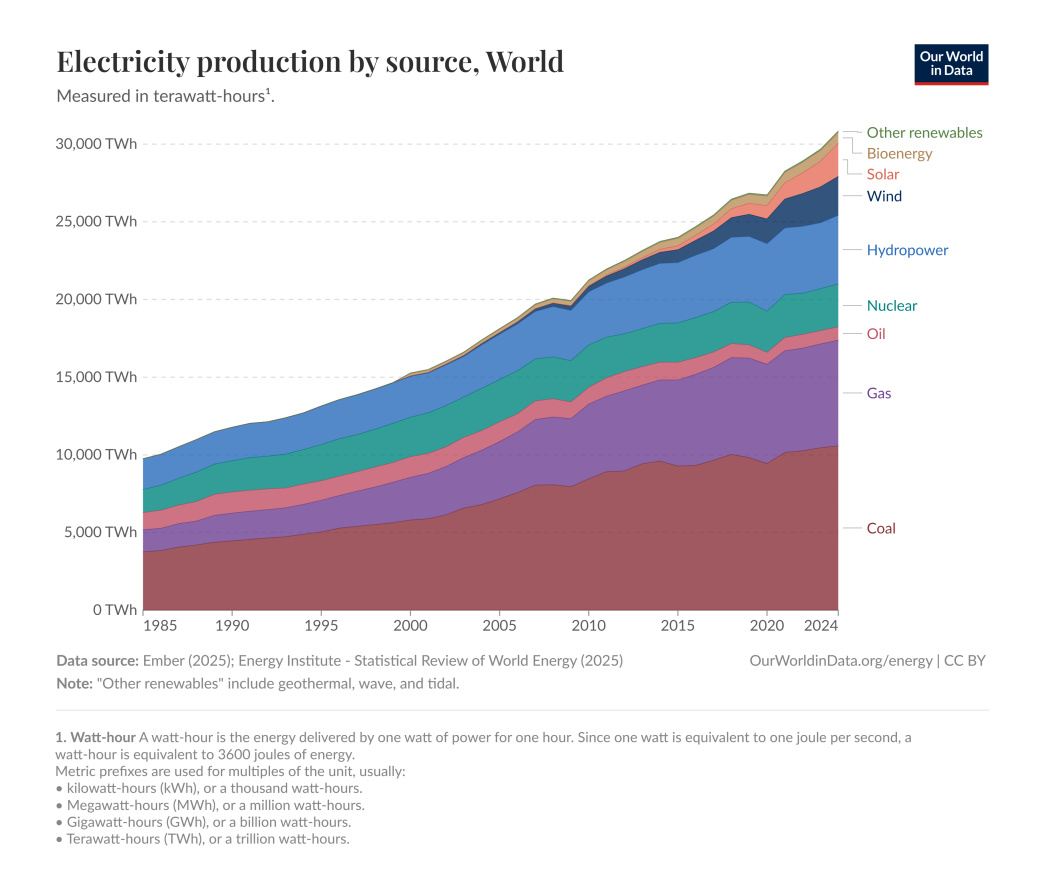


Figure 8: Electricity production with sector contributions [14]

1.2.8 White hydrogen

It is generated naturally within the Earth's crust from geochemical reactions between underground water and minerals. It is also called Natural hydrogen.

1.3 Hydrogen properties

In terms of fuel, comparisons are usually made with respect to other hydrocarbon fuels such as Methane (CH_4), principal constituent of natural gas, or Gasoline, a mixture of different hydrocarbons with a prevalence of heptane (C_7H_{16}). The higher the number of carbon atoms, the higher the molecular weight of the compound. Hydrogen has a higher heating value of 141.90 MJ/kg, way higher with respect to the 55.53 MJ/kg of methane and 47.50 MJ/kg of gasoline. Although, methane and gasoline are easier to be transported being in the liquid form at atmospheric conditions, with hydrogen being in the gaseous form. Because of this, it has to be stored as a pressurized gas or as a cryogenic liquid. Furthermore, it has a low volumetric energy density which creates challenges in storage and transport applications [15].

Hydrogen is colorless, odorless and tasteless, but it has a lower ignition concentration limit of 4%, which make it extremely dangerous in specific applications. When the hydrogen accumulates in oxygen and reaches a local concentration even of this percentage a spark ignites and explosion may happens. This aspect has to be monitored in applications, such as transportations and in fuel cells/electrolyser applications. Luckily. it has a good diffusivity in air, of around 0.61 cm2/s which makes difficult the previous dangerous concentration.

In the table below the main properties are summarized.

Property	Hydrogen	Methane	Gasoline
HHV (MJ/kg)	141.90	55.53	47.50
$HHV (MJ/m^3)$	11.89	39.82	
LHV (MJ/kg)	119.90	50.02	44.50
LHV (MJ/m^3)	10.05	35.88	195.80
Stoichiometric mixture in air (vol. %)	29.5	9.48	1.75
Flammability limits (vol. %)	4–75	5–15	1.4–7.6
Flame speed (cm/s)	295	41	40
Flame temperature (°C)	2045	1875	2200
Autoignition temperature (°C)	585	540	230-470
Detonation limits (vol. %)	18-59	6–13	1–3
Detonation velocity (km/s)	1.8	1.5	1.6
Minimum ignition energy in air (mJ)	0.02	0.29	0.24
Flame luminosity	low	medium	high

Table 1: Combustion properties of Hydrogen, Methane, and Gasoline.

It is evident that hydrogen seems a promising solutions for energy applications, even though it present some challenges that need to be faced.

This thesis will focus on hydrogen production through water electrolysis and electrolyser applications, with a section specifically related to green hydrogen production with its coupling to a photovoltaic plant.

To understand possibilities, challenges and parameters influencing the performance of the electrolyser, models are generally developed as a fundamental tool to predict possible outcomes and behaviour. Various models with different level of accuracy are widely present in the literature. The goal is to analyze and develop a realistic dynamic behaviour of an electrolyser, in particular a PEM electrolyser as it will be discussed in the next chapter, in order to introduce a higher level of realism in the performance of this kind of devices.

2 Theoretical Background

2.1 What is a water electrolyser?

A water electrolyser is an electrochemical device that is able to decompose water into hydrogen and oxygen through redox reactions thanks to the usage of direct electric current.

$$H_2O(l) \longrightarrow H_2(g) + \frac{1}{2}O_2(g)$$
 (1)

The Gibbs free energy of the reaction, at ambient temperature and pressure (25°C and 1 bar), is of

$$\Delta G^{\circ} = +237.1 \, \frac{\text{kJ}}{\text{mol}}$$

And it is positive because power is required for the reaction to take place.

Briefly, a cell is composed of an anode electrode, where the oxidation reaction occurs, and of a cathode electrode, where a reduction reaction occurs. During the oxidation reaction, a molecule looses electrons and a positive ion, or a new molecule, is generated, while during a reduction reaction there's an absorption of electrons and eventually a negative ion, or a new molecule, is generated. The electrons generated at the anode migrate through the current collector to the cathode. Due to this charge separation and recombination, it is possible to define a local voltage gradient both at the anode and at the cathode. A total voltage gradient across the cell, that in this thesis will be referred as "voltage of a single cell", can be considered as the difference of the two electrode's voltage gradient.

In between the electrodes there's an electrolyte layer, which allows the exchange of ions from one side to the other but not gas permeation. If it conduct positive ions, then after the oxidation at the anode there's the generation of positive ions and these are conducted from the anode to the cathode, where a new molecule will be formed. Instead, if it is able to conduct negative ions, the negative ions obtained at the cathode will be transported through the membrane to the anode and there a new molecule will be formed. The two possibilities depend on the material used for the electrolyte.

The input power can come from various sources as it was briefly mentioned in the previous chapter. The excess of power in the grid could be used as input power in electrolysers for hydrogen production activities, after its conversion from alternate to direct current. This option offers in addition a support to the grid in managing the unbalance between production and consumption. Otherwise, power could come from a direct couplt to a renewable energy source, such as solar, wind, hydro and geothermal power, without the intermission of the grid.

page 16 Master Thesis

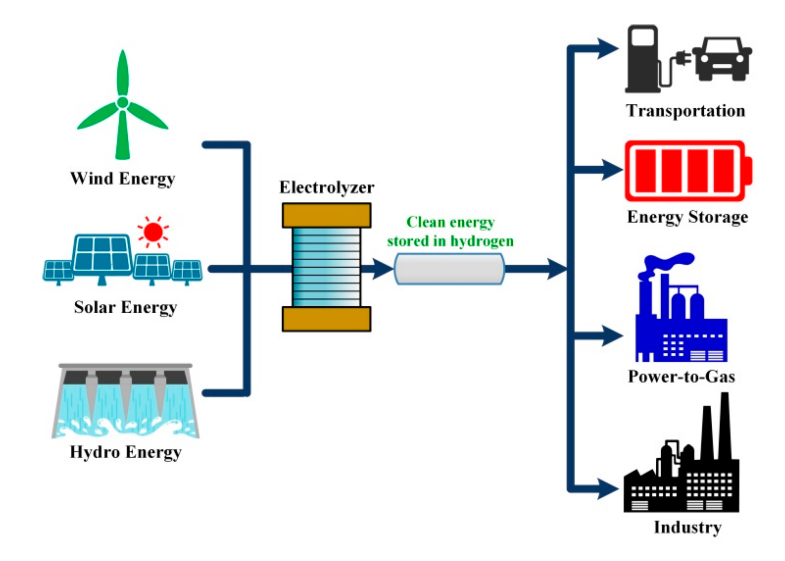


Figure 9: Renewable energy sources coupled to an electrolyser [16]

Water can come from industrial applications, such as smelting facilities, petroleum refineries or food processing industries, or from urban wastewater, such as municipal water, or groundwater. Although, the water used in the electrolyser has to respect high level of purities and several filtrations and treatments are conducted before its introduction in the device. Water can also come from cooling towers in the industry, from rain water, from surface water such as lakes or rivers or from the desalinization of sea water, which requires a high process cost. Researchers are trying to develop cells able to use sea water without desalinization, but the complex mixture that sea water represent introduces non negligible technical challenges to overcome [17].

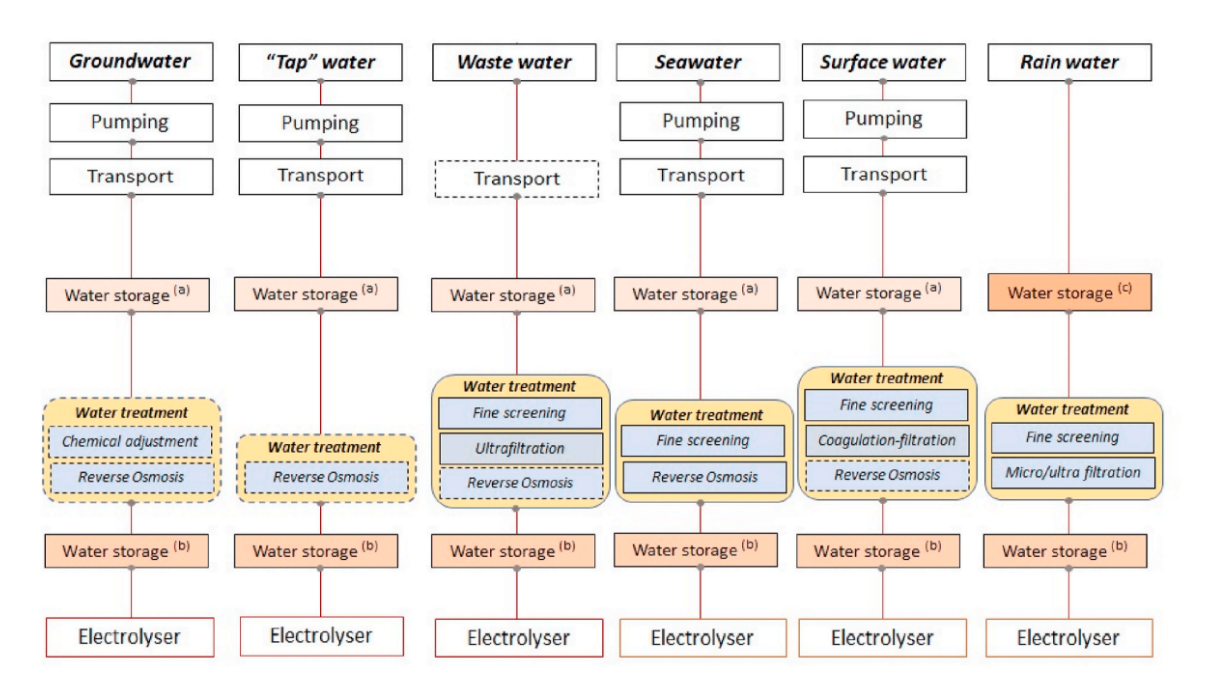


Figure 10: Water sources and treatments [18]

In a preliminar evaluation of a potential water source, apart from the cost associated to the treatment itself, it is necessary to account for all the costs associated to water pumping, transportation and storage before and after the chemical processes, which are strongly dependent on the site, the origin and the distance from the hydrogen production. In addition, water needed for the electrolysis cannot be considered equal to the stoichiometric value in the chemical balance, due to water losses during the various steps and to the need to keep hydrated the electrolyser membrane. It is possible to consider more or less 5% water losses during the extraction phase, 10% losses in transport, 15–40% during water treatments, 10% losses at the electrolyser input, 25% water in excess needed for cleaning and an additional 10% water for minimising shortage risks[18].

Furthermore, every water source has its own quality level and specific requirements, especially in particular to eventual pollutants that have to be monitored and removed. In fact, high quality hydrogen is necessary due to the eventual deposition of impurities on the electrode surfaces or on the membrane [18], as it will be mentioned in the next chapter specifically regarding electrocatalyst and catalyst degradation phenomena. Commercial electrolyser manufacturers typically specify a minimum required water supply quality in terms of conductivity, typically around $< 1~\mu S~cm^{-1}~(> 1~M\Omega~cm)$, and a total organic carbon (TOC) content [19].

Water is introduced at the anode or at the cathode depending on the type of electrolyser and on the ions that can permeate the membrane. Instead, the produced hydrogen is always generated at the cathode and through it gas diffusion layer exits the cell, with the oxygen generation happening at the anode.

To better understand the structure and the characteristic of an electrolyser, a detailed description of its components follows below:

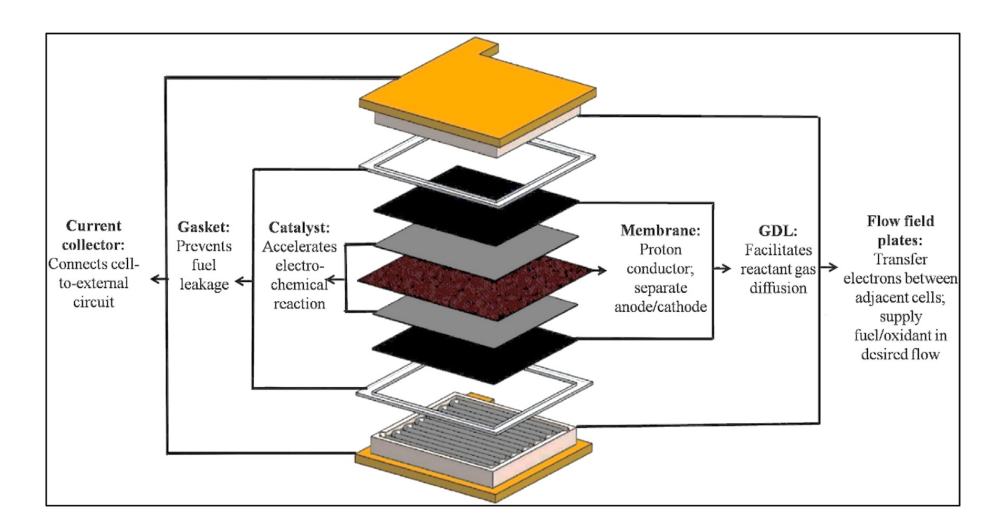


Figure 11: General scheme of an Electrolyser [20]

• Flow field plates: There are two types of electrolysers based on the polarity of the electrodes, which are monopolar with both electrodes either negative or positive with parallel electrical connection of the individual cells, or bipolar where the individual cells are connected in series. They have to simultaneously ensure charge carrier transport from cell to adjacent cell, supply and removal of reactants (i.e., water) and of produced gases. Additional functions include the facilitation of mass transport, both for reactants and products,

page 18 Master Thesis

and heat management through the presence of small flow channels used to let water flow wash over the gas diffusion layer and the remaining gases [21].

- Current collectors (CC): Current collectors are the components that collect the electrons, coming from the external circuit, next to the active surface of the electrodes. They also need to allow the movement of the water and of the gases involved.
- Gas diffusion layers (GDL): These layers are made of electrically and thermally conductive porous materials in which the components flow in and out.
- Catalyst coated membrane (CCM): The catalyst is used to enhance and accelerate the reaction. A catalyst layer is present both facing the anode and the cathode side, but the material differs based on the electrode's material used.
- Membrane: It keeps separated the product gases on the two sides but allows the transport of ions between the electrodes and supports the cathode and anode catalyst layer. A term usually considered in an electrolyser is MEA, membrane electrode assembly. Two possible versions of the MEA can be considered: three-layers MEA, which includes the internal membrane and the two catalyst layers , or five-layers MEA, which also includes the two Gas Diffusion Layers.
- **Gaskets**: They are used to seal layers of the cell to prevent gas leakages towards the outside, to maintain electrically insulation and to maintain system's pressure desired.

2.2 Types of water electrolysers

It is possible to consider four kind of electrolysers based on the electrolyte, operating temperature and pressure conditions and the type of ion permeating the membrane:

- 1. Alkaline water electrolyser (AEL)
- 2. Anion Exchange Membrane (AEM) water electrolyser
- 3. Proton Exchange Membrane (PEM) water electrolyser
- 4. Solid Oxide Water electrolyser (SOEL)

The first three electrolysers will be briefly discussed since they are not the main object of this thesis, while a dedicated fully described section will follow for the Proton Membrane Exchange electrolysers.

2.2.1 Alkaline water electrolyser

Alkaline water electrolysers are made of Asbestos/Zirfon/Nickel coated perforated stainless-steel diaphragms through which OH⁻ ions migrate from the cathode to anode side [22]. For the gas diffusion layer a nickel mesh/foam is used and stainless steel or nickel coated stainless steel separator plates are used for the plates. The electrolyte solution is an alkaline solution (KOH/NaOH).

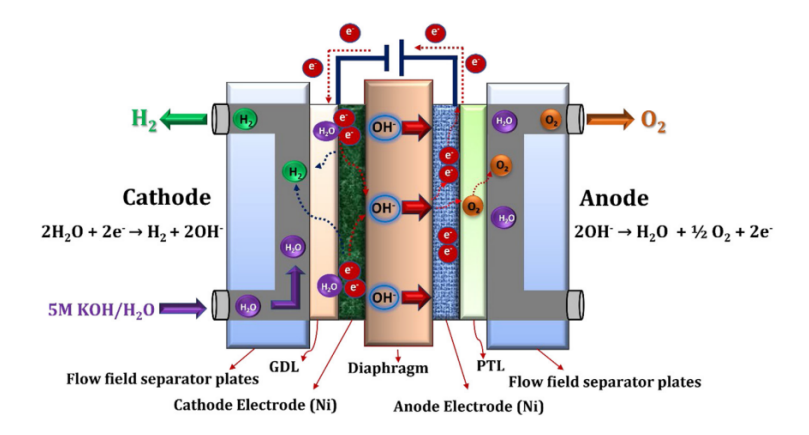


Figure 12: Alkaline water electroyser cell scheme [22]

These kind of electrolysers work with a lower range of temperatures, around 30° to 80° C and with low current densities (0.1–0.5 A/cm2) due to moderate OH⁻ mobility and the KOH electrolyte which is corrosive at high temperature. The voltage range limit is in between 1.4-3 V. The working pressures are lower than 30 bar in the cell and it has an efficiency of 50%–78%. Furthermore, they produce low purity gasses, with a level of purity of 99.9%.

2.2.2 Anion exchange membrane (AEM) water electrolyser

AEM electrolysers are made of a quaternary ammonium ion exchange membrane such as Sustanion®, Fumasep abd Fumatech. For the anode' electrode Nickel is the main used material, while both Nickel or NiFeCo alloy can be used for the cathode. For the gas diffusion layers, Ni foam/carbon cloths are used. Stainless steel and Ni-coated stainless steel are used instead for the bipolar plates [22].

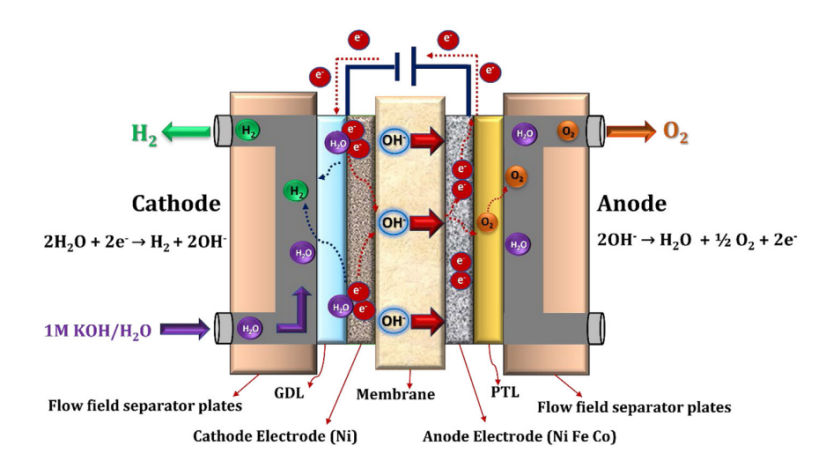


Figure 13: Anion exchange membrane water electrolyser cell scheme [22]

These kind of electrolysers still allow the conduction of OH^- ions from the cathode to the anode. The working temperature is around 40° - 60° C and the operating pressure of the cell is lower than 35 bar. They are capable to work in a wider range of current densities, from 0.2 to 2 A/cm2 and in a voltage range of 1.4-3 V.

page 20 Master Thesis

Right now, these electrolysers are still under development and are present in low sizes, in the range of kW. The current efficiencies are around 57%-59%.

2.2.3 Solid oxide water electrolyser

For the hydrogen electrode the main material is Ni-YSZ (Nichel-Yttria Stabilized Zirconia), which has a high electronic conductivity, and for the oxygen perovskite materials are used, such as LSCF ($\text{La}_{0.58}\text{Sr}_{0.4}\text{Co}_{0.2}\text{Fe}_{0.8}\text{O}_{3-\delta}$) and LSM ($\text{La}_{1-x}\text{Sr}_x$) $_{1-y}\text{MnO}_{3-\delta}$ [22]. The electrolyte is still YSZ and for the gas diffusion layer a Ni foam/mesh is used.

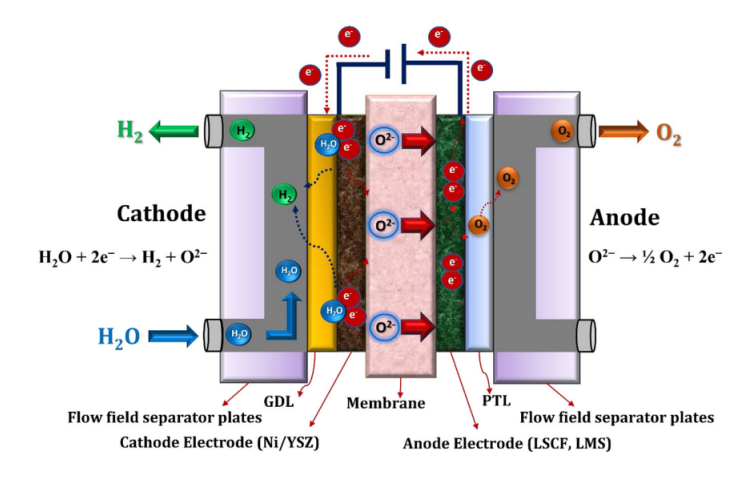


Figure 14: Solid oxide water electrolyser cell scheme [22]

These kind of electrolysers work at a high range of temperatures, around 700° - 850° C. Despite the rest of the electrolyser, the working pressure is of 1 bar. The current density range is of 0.3-1 A/cm2 and the voltage range is of 1.0-1.5 V. The efficiency is higher with respect to the other two, being around 89%

2.2.4 Proton Exchange Membrane (PEM) water electrolyser

The electrolysis reaction in a PEM can be decomposed in an Oxygen evolution reaction (OER) at the anode and in a Hydrogen evolution reaction (HER) at the cathode.

Anodic reaction:
$$H_2O \longrightarrow \frac{1}{2}O_2 + 2H^+ + 2e^-$$
 (2)

Cathodic reaction:
$$2 H^+ + 2 e^- \longrightarrow H_2$$
 (3)

Global reaction:
$$H_2O \longrightarrow H_2 + \frac{1}{2}O_2$$
 (4)

Water is inserted at the anode and when an electrical DC power source is connected to the electrodes and it is high enough, the decomposition of water starts. The electrons flow through the external circuit, flowing from the anode to the cathode, while the hydrogen protons flow through the permeable membrane from anode to the cathode.

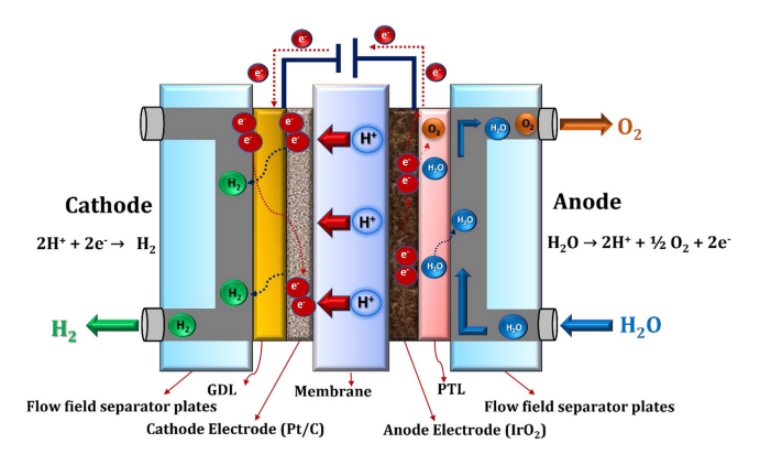


Figure 15: Proton Exchange Membrane (PEM) water electrolyser cell scheme [22]

With respect to the materials we have:

- Flowfield plates: bipolar plates are used. On the anode side, materials capable to resist to corrosion are needed due to the higher voltage of the electrode and usually titanium is used for the scope. Instead, titanium or graphite can be used on the cathode side, since the corrosion problem is not as prevalent as the anode's one [20].
- Current Collector (CC): for the anode highly corrosion-resistant materials need to be used, such as Titanium with surface coatings to avoid passivation. Instead, for the cathode stainless steel, Titanium or Graphite can be used.
- Gas Diffusion Layers (GDL): in a PEM, on the anode side water flows in and both a portion of remaining water and oxygen flows out, while hydrogen exits on the cathode side along with permeated water from the anode side. The components can flow only because of these channels and they are usually made of carbon paper or carbon cloth [20].
- **Membrane:** the internal proton exchange membrane allows the exchanges of H⁺ protons from the anode to the cathode side and for a PEM the membrane is usually made of NAFION, sulfonated tetrafluoroethylene based fluoropolymer-copolymer. The NAFION starts from a backbone of Teflon (CF₂)_n that is then modified adding a long side chain ending with an active ioni site SO₂⁻-H⁺. In its definition it is followed by a number indicating the thickness and the typology of the membrane (such as NAFION 117, 115, 221 etc...) [20].
- Catalyst Coated Membrane (CCM): since in a PEM electrolyser the membrane is made of NAFION and because it is delicate in terms of carbon cracking and temperature, a costly catalyst is used, with IrO2 on the anode side and Pt on the cathode's. The IrO2 has a high stability with respect to other materials such as Ru or RuO2. Most of the times a conductive support is used to increase the electric conductivity of the CCM, thus reducing the noble catalyst loading and cost. For the anode it is not mandatory but in case it is used, with a IrO2 or Ir catalyst oxides and ceramics such as TiO2 or SnO2 can be used as support materials. These catalyst supports should be anticorrosive and due to this condition titanium and its oxides are commonly used. Instead, when Pt is used at the

page 22 Master Thesis

cathode due to its high cost a conductive support is necessary and usually carbon materials can be used, with respect to the anode. In fact, due to the higher anodic potential (>1.5 V) the eventual use of carbon materials would lead very easily to the carbon's oxidation into carbon dioxide, reaction that already takes place at lower potential (around 0.206 V) [20].

• Gaskets: a typical material used is the Polytetrafluoroethylene [20].

3 Chemical degradation of a PEMWE

3.1 Types of degradations in a PEM

The degradation rate of a PEM is influenced by multiple factors, including environmental conditions, operational parameters, and material selection. These are outlined below:

- **Environment:** Conditions such as acidity levels and overpotential can lead to catalyst dissolution, membrane thinning, and bipolar plate passivation.
- Working conditions: Parameters like temperature, pressure, current density, power load cycles, and acidic solution concentration directly affect degradation behavior.
- **Material choices:** The selection of one material over another influences ion and electron migration, as each material has its own physical and chemical characteristics

The degradation process affects all components of the cell, but in different ways depending on their function and exposure.

3.1.1 Electrocatalyst and catalyst layer degradation

Catalyst degradation occurs slowly in time and initially it can be hard to detect it. In fact, the deposition and re-dissolution of catalyst particles could initially increase the catalyst activity not allowing for a fast and rapid detection. With time, though, the instable compounds originated would compromise the correct functioning of the electrolyser. An eventual degradation of the catalyst layer can be detected by changes in the catalyst activity or by a direct measure of the physicochemical properties of the catalyst.

For example, a common cause of dissolution for the catalyst is found in an increase of anodic and cathodic voltage. Considering IrO2 for the anode, around an anodic voltage of 1.8~V it begins to turn into Ir(OH)3 or IrO3, compounds known for their instability and high solubility at low Ph [23].

Furthermore, the increase of the voltage could lead to a catalyst layer disintegration and eventual agglomeration of Ir particles. This agglomeration, because of the increase of size of the catalyst particles, causes significant surface area losses and leads, as ultimate consequence, to the deactivation of the anode. Regarding the cathode, some report that Pt/C does not degrade until a cathodic potential higher than $0.4 \ V \ [23]$.

In case of platinum degradation, the migration of its particle to a region of the membrane close to the cathode would occlude the active surface sites and eventually lead to current reversal due to particles agglomeration.

The degradation of the catalyst layer furthermore enhances the increase of the anodic voltage, leading to a circular effect of cause and effect.

A possible external cause of increase of the anode and cathode's voltage is found in the presence of metallic cation impurities in the feeding water, coming from water pipes and stack components. The cations occupy ion exchange sites in the electrolyte membrane and in the catalyst layer and increase the charge transfer resistance, increasing then the voltages at the electrodes. Fortunately, this poisoning can be easily solved removing the MEA and cleaning it in liquid acid, washing away the impurities.

page 24 Master Thesis

In addition, the morphology of the catalyst contributes to the eventual degradation. For example, thin film electrodes are reported to be less sensitive to agglomeration and corrosion [23].

In the end, it is important to ensure a tight attach of the catalyst layer to the support and the membrane. To increase the attachment, surface etching methods could be used to increase the membrane roughness and then the adherence to the catalyst layer, although leading to a decrease of the membrane's mechanical strength.

3.1.2 Membrane degradation

The NAFION membrane of the PEM is the weakest component of the elctrolyser in terms of long term performance. Its degradation is particularly important because it may lead to a recombination of the hydrogen and the oxygen and then to H2 and O2 crossover. This phenomenon has been investigated in a dedicated section in the sixth chapter.

Mechanical degradation can happen due to compressive forces exercised by the bipolar plates that sandwich the membrane. The compression is done in order to avoid the exits of the gasses, but micro fractures can be originated due to these compressions. In addition, the increase of the roughness of the membrane as a result of the increase of the adhesion of the catalyst layer could lead to a decrease of membrane's durability.

Thermal degradation is also an important source to consider. The working temperature of the PEMs is around 60°-80°C, but due to the heat generated during the electrolysis a gradient of temperature is present across the cell and the MEA's temperature is relatively higher with respect to the rest of the stack. This could lead to hot spots formations and consequent micro cracks through the membrane. A correct thermal menagement is important to avoid hot spots formation and the sudden increase of temperature in the electrolyser.

The introductions of new materials for the membrane such as polyetheretherketone (PEEK), polysulfone (PSF), and polybenzimidazole (PBI) could lead to a lower production cost and a higher resistance to higher temperatures, reducing the risk of thermal degradation. AquivionTM from "Solvay" shows a wide operating temperature range (up to 150° C), good resistance to gas crossover and reduced mechanical degradation under high pressure operation [23].

Chemical degradation is originated as a consequence of the degradation of the hydrogen and oxygen crossover through the membrane. After internal recombination, compounds such as hydrogen peroxide (H_2O_2) , hydroperoxyl radical (HO_2) and hydroxyl radical (HO) are created and will additionally attack the membrane leading to fluoride and sulfur release. This kind of degradation can be actually measured measuring the fluoride release rate (FRR) and the sulfur emission rate (SER) [23]. Since gas crossover normally occurs in small quantities in the cell, a correspondent little amount of the previously mentioned compounds is normally present but its amount can vary with respect to the increase of working temperature and current density.

The usage of thicker or more compressible cathode layers could also be a solution especially regarding the gasses crossover, even if this could lead to the increase of ohmic drops across the MEA [23].

3.1.3 Bipolar plates degradation

In the case of bipolar plates, corrosion is the main concern that could affect the plates integrity and durability. When the anode plate is in contact with the produced oxygen, due to the higher anodic potential, titanium is oxidized producing titanium ions that reacts with the produced oxygen and precipitates as TiO2. As a consequence, a thin layer of TiO2 is formed on the surface, increasing the isolation and thus increasing contact resistance. This phenomenon is also referred as "passivation". Furthermore, in the case of fluoride release, coming from the membrane due to its eventual degradation, a reaction with the TiO2 compound could occur.

$$TiO_2 + 4H^+ + 6F_{aq}^- \longrightarrow [TiF_6]^{2-} + 2H_2O$$
 (5)

The titanium-fluorine ions remain in circulations and can interfere with the membrane occluding the passages.

3.1.4 Current collectors degradation

Regarding the current collectors, chemical and mechanical degradations are usually considered.

Chemical degradation is due to corrosion phenomena which mainly involve the Titanium used at the anode. In acidic conditions, such as the anodic ones, titanium can be corroded and fluoride ions coming from membrane degradation can attack the TiO_2 layer and generate $Ti-F^-$ compounds [23]. Titanium can also be attacked by hydrogen peroxide resulting from hydrogen crossover and causing titanium ions release in the solution.

These phenomena are similar as the ones previously mentioned for the bipolar plates and, as for them, coatings are used for the collectors in order to obtain a good oxidation resistance.

In terms of Mechanical degradation, the high compression forces mainly affect the the gas and water permeability but at the same time they improve the contacts and reduce the ohmic resistances.

4 Mathematical model

The developed model follows a chemical-thermal approach in order to reproduce as realistically as possible the behavior of a PEM electrolyser. An initial base model is developed using the basic equations commonly applied in some already existing models and some implementations are introduced later to reflect more realistically the real operating of the system.

To validate the results and demonstrate the improved realism of the developed model, an equivalent electrical model of the electrolyser is implemented, how it will be shown later in Paragraph 6.3.

The model is simulated in the Matlab/Simulink® environment and it is composed of four main blocks: Anode, Cathode, Membrane and Voltage. Furthermore, a thermodynamic block is present to simulate the thermal behaviour of the electrolyser. All the blocks are interconnected and outputs of a block are used as inputs for others.

The PEM electrolyser analyzed is a Pt anode and cathode electrolysed based with a NAFION 117 membrane.

The overall configuration is represented below.

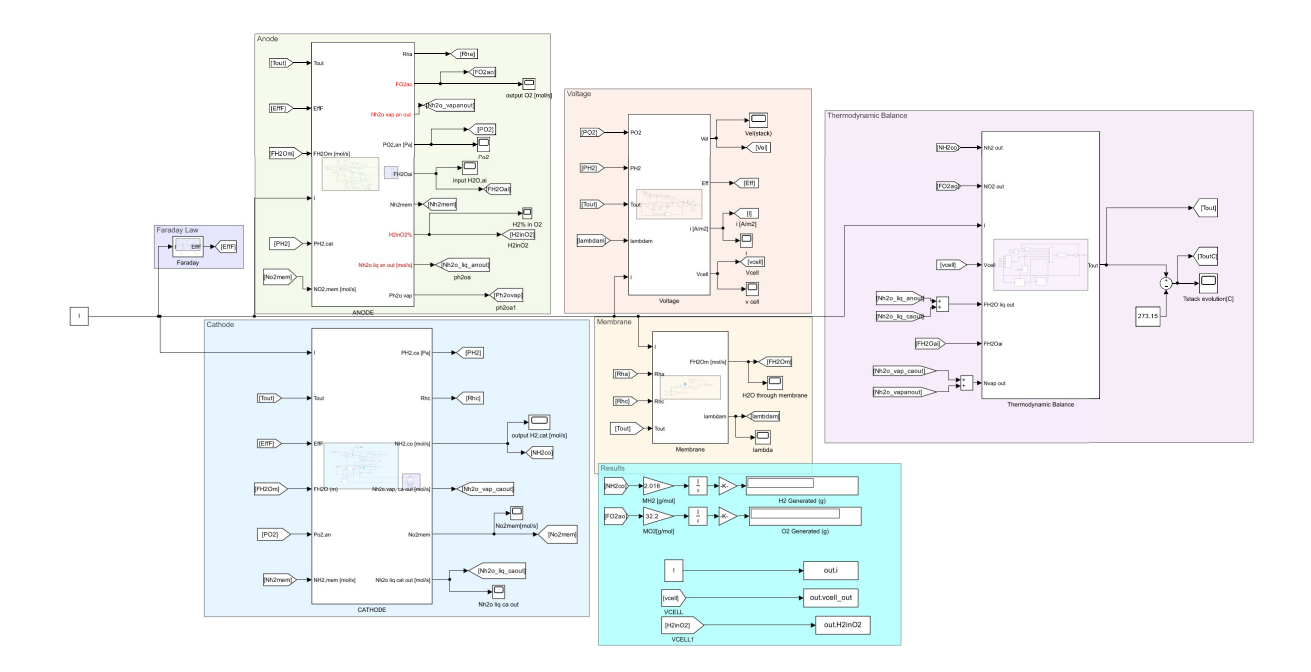


Figure 16: Electrolyser general scheme blocks

4.1 Anode

In the anode, the partial reaction that takes place is the following one:

To simulate the dynamic inside the anode, two mass balances are considered:

$$\frac{dN_{H_2O,an}}{dt} = N_{H_2O.in} - N_{H_2O.memb} - N_{H_2O.an,out}$$
 (6)

page 28 Master Thesis

where:

• $N_{\text{H}_2\text{O},\text{an}_{in}}$ is the input molar flow rate of water in the anode [mol/s]. It is calculated considering the Faraday law and an excess of water, expressed by λ , in order to keep the membrane hydrated and to guarantee the cooling effect carried by the water of the cell itself. The following expression is considered:

$$N_{\text{H2O}_2,\text{an in}} = \frac{n \cdot I}{F \cdot 2} \cdot \eta_{\text{eff}} \cdot l \quad [\text{mol/s}]$$
 (7)

where:

- *I*: electric current supplied to the cell [A]
- n: number of cells
- 2: number of electrons transferred per mole of substance
 - * for hydrogen and water: n = 2
 - * for oxygen: n = 4
- F: Faraday constant ($F = 96485 \,\mathrm{C/mol}$)
- $\eta_{\rm eff}$: Faraday efficiency, which can be expressed as:

$$\eta_{\text{eff}} = \frac{i - i_{\text{loss}}}{i} \tag{8}$$

Where i_{loss} is estimated to be equal to 1% of the current density.

- *l*: coefficient expressing water in excess [-]
- $N_{\rm H_2O,mem}$ refers to the molar flow rate of water through the membrane, from anode to cathode [mol/s]
- $N_{\text{H}_2\text{O},\text{an_out}}$ refers to the molar flow rate of water going out from the anode [mol/s]

Instead, for the Oxygen Balance:

$$\frac{dN_{\rm O_2}}{dt} = N_{\rm O_2,gen} - N_{\rm O_2,out} \tag{9}$$

Where:

• $N_{O_2,gen}$ is the oxygen generated, calculated via Faraday's law:

$$N_{\text{O}_2,\text{gen}} = \frac{n \cdot I}{F \cdot 4} \cdot \eta_{\text{eff}} \quad [\text{mol/s}]$$
 (10)

ullet $N_{
m O_2,out}$ is the molar flow rate of oxygen exiting from the anode.

An initial hypothesis assumes that both O_2 and H_2O behave as ideal gases. Therefore, the ideal gas law is used to compute partial pressures, considering the evolving temperature of the cell and the moles in the electrode:

$$P_{\mathcal{O}_2} = \frac{n_{\mathcal{O}_2, \mathrm{an}} \cdot R \cdot T}{V_{\mathrm{an}}} \quad [\mathrm{Pa}] \tag{11}$$

Where:

- *T*: stack temperature [K]
- *R*: universal gas constant [J/mol·K]
- V_{an} : volume of the anode [m³]
- $n_{O_2,an}$: moles of oxygen at the anode [mol]

Similarly, for water:

$$P_{\text{H}_2\text{O,an}} = \frac{n_{\text{H}_2\text{O,an}} \cdot R \cdot T}{V_{\text{an}}} \quad [\text{Pa}]$$
 (12)

The pressure at the anode is given by the sum of the partial pressures:

$$P_{\rm an} = P_{\rm O_2,an} + P_{\rm H_2O,an}$$
 [Pa] (13)

And then, the molar fraction can be obtained as the ratio between the partial pressure of the components and the total pressure at the anode:

$$y_{O_2} = \frac{P_{O_2}}{P_{\rm an}} \tag{14}$$

$$y_{\rm H_2O,an} = \frac{P_{\rm H_2O,an}}{P_{\rm an}} \tag{15}$$

And, considering that the total outlet molar flow can be expressed through the following formula:

$$N_{\text{an out}} = k_{\text{ao}} \cdot (P_{\text{an}} - P_{\text{el}}) \quad [\text{mol/s}] \tag{16}$$

Where:

- k_{ao} : anode outlet flow coefficient [mol/s·Pa]
- $P_{\rm el}$: external standard pressure [Pa]

Then, the molar fractions are applied to obtain the singular outlet molar flows:

$$N_{\text{H}_2\text{O},\text{an}_-\text{out}} = y_{\text{H}_2\text{O},\text{an}} \cdot N_{\text{an}_-\text{out}} \quad [\text{mol/s}]$$
(17)

$$N_{\text{O}_2,\text{out}} = y_{\text{O}_2,\text{an}} \cdot N_{\text{an_out}} \quad [\text{mol/s}]$$

$$\tag{18}$$

page 30 Master Thesis

4.2 Cathode

At the cathode, similar considerations have been done for the hydrogen content and water content. Considering the following partial reaction:

The differential equations used for H₂ and H₂O are the following:

$$\frac{dN_{\rm H_2}}{dt} = N_{\rm H_2,gen} - N_{\rm H_2,out} \quad [\text{mol/s}] \tag{19}$$

The generated moles of hydrogen can be calculated through Faraday's law:

$$N_{\rm H_2,gen} = \frac{n \cdot I}{2 \cdot F} \cdot \eta_{\rm eff} \quad [\text{mol/s}]$$
 (20)

For the water content:

$$\frac{dN_{\text{H}_2\text{O,ca}}}{dt} = N_{\text{H}_2\text{O,mem}} - N_{\text{H}_2\text{O,cat,out}}$$
 (21)

The water arriving at the cathode will be discussed in the membrane section. Again, it is possible to calculate the partial pressure for the two using the Ideal Gas Law:

$$P_{\rm H_2} = \frac{n_{\rm H_2} \cdot R \cdot T}{V_{\rm ca}} \quad [\rm Pa] \tag{22}$$

$$P_{\text{H}_2\text{O,ca}} = \frac{n_{\text{H}_2\text{O,ca}} \cdot R \cdot T}{V_{\text{ca}}} \quad [\text{Pa}]$$
 (23)

$$P_{ca} = P_{H_2} + P_{H_2O,ca}$$
 [Pa] (24)

$$y_{\rm H_2O,ca} = \frac{P_{\rm H_2O,ca}}{P_{\rm ca}}$$
 and $y_{\rm H_2} = \frac{P_{\rm H_2}}{P_{\rm ca}}$ (25)

The outlet molar flow that exits from the cathode is calculated similarly to the anode case:

$$N_{\text{cat out}} = K_{\text{co}} \cdot (P_{\text{cat}} - P_{\text{el}}) \tag{26}$$

Then, the individual molar flows are:

$$N_{\text{H}_2\text{O,ca}} = y_{\text{H}_2\text{O,ca}} \cdot N_{\text{cat out}} \quad [\text{mol/s}] \tag{27}$$

$$N_{\text{H}_2,\text{ca}} = y_{\text{H}_2} \cdot N_{\text{cat out}} \quad [\text{mol/s}] \tag{28}$$

4.3 Membrane

The H+ ions obtained from the partial reaction at the anode are then transported through the membrane to the cathode side where the HER, hydrogen evolution reaction, happens. Nevertheless, even if water is introduced at the anode side, some molecules are transported thought the membrane due to three main phenomena: electro-osmotic drag, diffusion and hydraulic pressure effect. Commonly, it is possible to focus the treatise considering only the electro osmotic drag and the diffusion term, neglecting the hydraulic pressure one due to the higher influence that the other two terms have with respect to it [24].

Then, it is possible to consider that the water molar flow through the membrane can be calculated as:

$$N_{\text{H}_2\text{O,mem}} = N_{\text{H}_2\text{O,diff}} + N_{\text{H}_2\text{O,eod}}$$
 (29)

Where $N_{\rm H_2O,diff}$ refers to the diffusion phenomenon. It is due to concentration gradient between the anode and the cathode and can be calculated using the Fick's law of diffusion:

$$N_{\rm H_2O,diff} = D_w \cdot \left(\frac{C_{\rm wc} - C_{\rm wa}}{t_{\rm me}}\right) \cdot A \quad [\rm mol/s] \tag{30}$$

Where:

• C_{wc} and C_{wa} are the water concentration at the cathode and at the anode, which can be calculated through the density of the membrane at the dry state (ρ_{me}) , the equivalent weight (EW) of the membrane and the anode and water content (λ_{an}) and (λ_{cat}) :

$$C_{\rm wc} = \frac{\rho_{\rm me}}{\rm EW} \cdot \lambda_{\rm cat} \qquad C_{\rm wa} = \frac{\rho_{\rm me}}{\rm EW} \cdot \lambda_{\rm an}$$
 (31)

The water content of the anode and cathode can be calculated through the water activities at the two electrodes, $a_{\rm an}$ and $a_{\rm cat}$, which depend on the water partial pressure and the saturation pressure of the water at the given temperature of operation. Water activities are expressed as relative humidities due to the previous hypothesis of ideal gas mixture behaviour:

$$a_{\rm an} = \frac{P_{\rm H_2O,an}}{P_{\rm sat}} \qquad a_{\rm cat} = \frac{P_{\rm H_2O,cat}}{P_{\rm sat}} \tag{32}$$

An empirical formula is used for the calculation of the saturation pressure [25]:

$$P_{\text{sat}}(T \, ^{\circ}\text{C}) = -2846.4 + 411.24 \cdot T - 10.554 \cdot T^2 + 0.16636 \cdot T^3 \text{ [Pa]}$$
(33)

with T being the working Temperature of the electrolyser.

Then, it is possible to make the calculation based on the water activities. The calculations are conducted both for anode and cathode:

$$\lambda_i = \begin{cases} 0.43 + 17.18 \cdot a_i - 39.85 \cdot a_i^2 + 36 \cdot a_i^3 & \text{se } 0 < a_i \le 1\\ 14 + 1.4 \cdot (a_i - 1) & \text{se } 1 < a_i \le 3 \end{cases}$$
(34)

Although, in order to simplify the order of complexity of the model, considering a range of 14 to 25, a general value of 20 has been used for the water content of the electrolyser, as commonly considered in various literature examples [24].

page 32 Master Thesis

• D_w is the water diffusion coefficient in the membrane [m²/s]. it can be calculated based on the temperature of the cell and the membrane water content:

$$D_{\lambda} = \begin{cases} 10^{-10} & \lambda_{m} \leq 2\\ 10^{-10} \cdot (1 + 2 \cdot (\lambda_{m} - 2)) & 2 < \lambda_{m} \leq 3\\ 10^{-10} \cdot (3 - 1.76 \cdot (\lambda_{m} - 3)) & 3 < \lambda_{m} \leq 4.5\\ 1.25 \cdot 10^{-10} & 4.5 < \lambda_{m} \end{cases}$$
(35)

Where the membrane water content can be calculated considering the mean value of the water content at the anode and at the cathode,

- t_{me} is the membrane thickness [m],
- A is the membrane area [m^2].

Instead, the electro osmotic drag can be calculated as follows:

$$N_{\rm H_2O,eod} = \frac{n_d \cdot i \cdot A}{F} \quad [\text{mol/s}] \tag{36}$$

where the electro osmotic drag coefficient can be considered as a function of the membrane water content:

$$n_d = 0.0029 \cdot \lambda_m^2 + 0.05 \cdot \lambda_m - 3.4 \cdot 10^{-19} \tag{37}$$

4.4 Voltage of the cell

Considering to work at specific operating conditions, such as a specific T and pressure, a minimum voltage is required to start the electrolysis. It is defined as the "reversible voltage" or Nernst Voltage and it is calculated through the Nernst equation that can be expressed as follows:

$$V_{\text{rev}} = E_0 + \frac{RT}{2F} \ln \left(\frac{p_{\text{H}_2} \sqrt{p_{\text{O}_2}}}{p_{\text{H}_2\text{O}}} \right)$$
 (38)

where:

- $p_{\rm H_2}$: partial pressure of hydrogen at the cathode side [Pa]
- p_{O_2} : partial pressure of oxygen at the anode side [Pa]
- $p_{\rm H_2O}$: partial pressure of H2O (if the water is considered all in liquid form the water activity a=1 is considered instead) [Pa]
- *E*₀: cell reversible voltage in standard conditions [V]

E0 can be calculated using the Gibbs free energy:

$$E_0 = \frac{\Delta G}{2 \cdot F} \quad [V] \tag{39}$$

However, in this model a correlation with respect to the temperature has been used, as follows:

$$E_0 = 1.5241 - 1.2261 \cdot 10^{-3} \cdot T + 1.1858 \cdot 10^{-5} \cdot T \cdot \ln T + 5.6692 \cdot 10^{-7} \cdot T^2$$
 (40)

With T being the temperature at which the electrochemical reaction occurs [24]. The second part of the expression of the reversible voltage express the deviation from standard conditions due to the pressure and the temperature variations in the cell.

However, the reversible voltage is the minimum voltage required to start the reaction, but in reality, several voltage drops inside the cell happens due to internal phenomena, and a higher voltage is required. The total cell voltage is then defined taking into consideration these internal overvoltages:

$$V_{\text{cell}} = V_{\text{rev}} + V_{\text{act}} + V_{\text{ohm}} + V_{\text{diff}} \tag{41}$$

where:

- \bullet $V_{
 m diff}$: it is the diffusion overvoltage. It is due to mass transport and concentration gradient between the anode and the cathode. Its contribution can be neglected in the case of PEM electrolysers as the applied current densities are not too high and the mass-transport limitation is unlikely to happen at the interface of the membrane and electrodes.
- V_{act}: activation overvoltage. It is related to the electrochemical reactions that happen over
 the electrodes and considers the energy required to activate the electrochemical reactions
 inside the anode and the cathode. The Butler–Volmer equation is used to express the
 activation overvoltage, both for the anode and the cathode.

$$V_{\rm act} = V_{\rm act,an} + V_{\rm act,ca} \tag{42}$$

$$V_{\text{act,an}} = \frac{RT}{\alpha_{an}F} \cdot \operatorname{arcsinh}\left(\frac{i}{2 \cdot i_{0,an}}\right)$$

$$V_{\text{act,cat}} = \frac{RT}{\alpha_{cat}F} \cdot \operatorname{arcsinh}\left(\frac{i}{2 \cdot i_{0,cat}}\right)$$
(43)

- α_{an} and α_{ca} : charge transfer coefficients [-]
- j: current density [A/m²]
- $j_{0,an}$ and $j_{0,ca}$: exchange current density of the anode and cathode [A/m²]

With the following formula for the exchange current density:

$$j_{0,\text{an}} = j_{0,\text{an-ref}} \exp\left[-\frac{E_{\text{act}}}{R} \left(\frac{1}{T} - \frac{1}{T_{\text{ref}}}\right)\right]$$
(44)

$$j_{0,\text{ca}} = j_{0,\text{ca-ref}} \exp \left[-\frac{E_{\text{act}}}{R} \left(\frac{1}{T} - \frac{1}{T_{\text{ref}}} \right) \right]$$
 (45)

page 34 Master Thesis

Where Eact is the activation energy of the electrodes and $j_{0,\text{an-ref}}$ and $j_{0,\text{ca-ref}}$ are the reference exchange current densities of the anode and the cathode, respectively. The considered range for the exchange current densities is between 10^{-11} - 10^{-4} A/m² for the anode, and between 10^{-6} - 10^{-1} A/m² for the cathode [26].

To simplify the calculations, a value of 10^{-12} A/cm2 is considered for the anode and a vlue of 10^{-3} A/cm2 for the cathode.

 \bullet V_{ohm} : Considering that in a cell two types of charged species are present, ions migration and electrons conduction, we should consider two contributions to the ohmic overvoltage (ionic and electronic). However, since the electronic resistivity is orders of magnitude lower than the ionic one, we will only consider the contribution given by the ionic resistance through the membrane:

$$V_{\text{ohm}} = R_{\text{ohm,i}} \times j \tag{46}$$

With j in [A/m2] and Rohm in $[\Omega]$. It can be expressed as the ratio of the thickness of the membrane and the membrane conductivity, which can be expressed as a dependence with respect to the temperature of the cell and the water content of the membrane:

$$R_{\text{ohm,i}} = \frac{\delta_{\text{mem}}}{\sigma_{\text{mem}}} \tag{47}$$

$$\sigma_{\text{mem}} = (0.514\lambda_{\text{mem}} - 0.326) \cdot \exp\left[1268\left(\frac{1}{303} - \frac{1}{T}\right)\right] \quad [\text{S/m}]$$
 (48)

From the voltage of the cell, it is possible to calculate the cell efficiency as the ratio of the thermoneutral voltage and the one of the cell:

$$\eta_{\rm el} = \frac{V_{\rm th}}{V_{\rm cell}} \tag{49}$$

The thermoneutral voltage is the voltage at which water electrolysis occurs without any heat exchange with the surroundings, meaning the process is thermally neutral. It separates the zone of exothermic and endothermic behaviour for an electrolyser and it can be expressed as follows:

$$V_{\rm th} = \frac{\Delta H}{2 \cdot F} \tag{50}$$

 ΔH is the enthalpy change of the water-splitting reaction, expressed in kJ/mol. A value of 1.481 V for the thermoneutral voltage has been considered in the calculations

In the end, since the model refers to a stack made of n cells, considered connected in series, the same current pass through all the cells but the voltage of the stack has to be considered as the product of the voltage of a single cell and the total number of cells, considering to have same behavior and material characteristics:

$$V_{\text{stack}} = V_{\text{cell}} \cdot n \tag{51}$$

4.5 Thermal block

In this section, the thermal behavior of the electrolyser is analyzed. Considering the whole stack as our control volume, it is possible to write the energy balance in the following way:

$$\frac{dE}{dt} = \dot{Q}_{\text{gen}} - \dot{Q}_{\text{loss}} - \dot{Q}_{\text{cool,tot}} + \sum (\dot{m}_i \cdot h_i)_{\text{in}} - \sum (\dot{m}_i \cdot h_i)_{\text{out}}$$
 (52)

Where the variation of the internal energy of the electrolyser in time depends on:

- the generated heat due to the electrical power of the electrolyser, $\dot{Q}_{
 m gen}$,
- ullet the losses due to exchange of heat between the stack and the environment, \dot{Q}_{loss} ,
- the energy associated to the input flows that go inside the control volume and the output ones that exits
- the heat needed to be removed to maintain the temperature of the electrolyser at the desired range.

The first term, the energy variation with respect to time, can be explicated as follows:

$$\frac{dE}{dt} = \frac{d\left(c_{pi} \cdot V_i \cdot \rho_i \cdot T\right)}{dt} \quad [W]$$

- V_i : electrolyser's volume [m³]
- $c_{p,i} = c_{p,H_2O}$: heat capacity of water, considered constant during the operation of the component $[J/(\text{mol}\cdot K)]$
- $\rho_i = \rho_{\rm H_2O}$: density of water, also considered constant [g/m³]
- *T*: stack temperature [K]

After these considerations, only the temperature is subjected to changes in time, so the previous equation can be simplified as follows:

$$\frac{dE}{dt} = c_{p,H_2O} \cdot V \cdot \rho_{H_2O} \cdot \frac{dT}{dt} \quad [W]$$
 (54)

The heat generated in the electrochemical process can be expressed considering the voltage of the cell, the thermoneutral voltage and the current flowing in the stack, taking into consideration the whole stack:

$$\dot{Q}_{\text{gen}} = N_c (V_{\text{cell}} - V_{\text{th}}) I \tag{55}$$

Then, since the electrolyser usually works at a temperature higher than the ambient one, it exchanges heat with the environment through the following formula:

$$Q_{\text{loss}} = Q_{\text{conv}} + Q_{\text{rad}} = (h_c + h_r) \cdot A_{\text{ext}} \cdot (T - T_{\text{env}}) \quad [W]$$
 (56)

The heat dissipated is due to convection and radiation phenomena.

page 36 Master Thesis

- A_{ext} : total external surface area of the stack [m²]
- h_c : convective heat transfer coefficient [W/(m²·K)]

• h_r : radiative heat transfer coefficient $[W/(m^2 \cdot K)]$

Where:

$$h_c = \frac{Nu \cdot k_m}{L} \tag{57}$$

The conductive heat transfer coefficient can be calculated considering the Nusselt Number Nu, the thermal conductivity $k_{\rm m}$ and the electolyser length L. For it is considered to exchange heat with the air, a value of 0,026 W/(m*K) is considered for $k_{\rm m}$. For the Nusselt number, considering the stack as a rectangular block exchanging heat with slow moving air and considering Re=5000 and Pr=0,7, it can be calculated as follows:

$$Nu = 0.66 \cdot Re^{0.675} \cdot Pr^{1/3} \tag{58}$$

Instead, for the radiative heat transfer coefficient:

$$h_r = 4 \cdot \varepsilon \cdot \sigma \cdot T_m^3 \quad \left(\frac{W}{m^2 \cdot K}\right) \tag{59}$$

- ε : emittance of the material ($\varepsilon = 0.6$ for rough stainless steel)
- σ : Stefan–Boltzmann constant ($\sigma = 5.67 \times 10^{-8} \, \mathrm{W/(m^2 \cdot K^4)}$)
- T_m : mean temperature between the stack and the environment.

Regarding the energy associated to the input and output molar flows we have the following expressions:

$$\sum (\dot{m}_i \cdot h_i)_{\rm in} = \dot{m}_{\rm H_2O_{ain}} \cdot h_{\rm H_2O_{ain}} \quad [W]$$
 (60)

Nevertheless, since it is necessary to impose a reference Temperature and pressure, 25°C and 1 bar are considered as standard condition, and because of that the enthalpy at standard condition is considered as the reference and then is assumed equal to zero.

Instead, at the output we have three flows, in which $m_{\rm H2O,out}$ considers both the water output at the anode and the cathode. The exiting conditions considered are based on $T_{\rm out}$ calculated in the model and for oxygen and hydrogen the expression considered to calculate the enthalpy makes reference to ideal gas considerations.

$$\sum (\dot{m}_i \cdot h_i)_{\text{out}} = \dot{m}_{\text{H}_2\text{O,cout}} \cdot h_{\text{H}_2\text{O,cout}} + \dot{m}_{\text{H}_2,\text{cout}} \cdot h_{\text{H}_2,\text{cout}} + \dot{m}_{\text{O}_2,\text{cout}} \cdot h_{\text{O}_2,\text{cout}} \quad [\text{W}] \quad (61)$$

In the end, considering the need to keep the electrolyser at an acceptable working temperature, and considering that the input water in the electrolyser is itself used to cool down the electrolyser, the following formula can be used to simulate a passive cooling:

$$Q_{\text{cool,pass}} = \dot{m}_{\text{H}_2\text{O}_{\text{in}}} \cdot c_{p,\text{H}_2\text{O}} \cdot (T_{\text{out}} - T_{\text{w,in}})$$
(62)

For this reason, we work with excess water at the input in order to satisfy the cooling effect and keep the desired working T.

Nevertheless, during the simulations it was clear that a natural passive cooling could work only for low values of current, while for higher current densities the temperature was reaching higher values with respect to the target one. Then, it was needed to introduce an active cooling effect simulated with an external circuit in which water is circulated through the cooling channels in order to subtract the excess of heat produced, keeping the Temperature around the target value.

Because of that, the following implementation has been considered:

$$Q_{\text{cool,att}} = \begin{cases} 0, & \text{if } T < T_{\text{ref}} \\ \dot{m}_{\text{ext}} \cdot c_{p,\text{H}_2\text{O}} \cdot (T - T_{\text{ref}}), & \text{if } T \ge T_{\text{ref}} \end{cases}$$
(63)

Where:

- $Q_{\text{cool,att}}$: heat removed actively [W]
- $\dot{m}_{\rm ext}$:external water mass flow used for cooling purposes [kg/s]
- c_{p,H_2O} : specific heat capacity of liquid water [J/kg·K]
- *T*: stack temperature [K]
- T_{ref} : target temperature

This formulation takes in consideration an external circuit directly used for cooling purposes in order to simplify the approach of the model, trying to simplify the real temperature control performed in a cell. From the summation of the two cooling effect we obtain the total one expressed in the Equation 52.

5 Part I: Implemented model

The previous model, although based on the fundamental equations used to represent the behavior of a general PEM electrolyser, it contains some limitations and forced hypothesis. In this section, some implementations have been developed in order to make the model more realistic and to simulate a more correct behavior of the stack.

Firstly, the modeling of the water moles within the cell was refined. The previous utilized formulas were referring to water as an ideal gas when calculating its partial pressure, even though the inlet water at the electrode is naturally in the liquid state. As a consequence, a reasoning about the pressures and the moles at both electrodes has been conducted.

Secondly, an implementation regarding a more realistic dynamic behavior of the stack with respect to variations of the input current was introduced. Switching from a constant input current to a variable one, it is not accurate to consider a sudden fast change of voltage without accounting for internal phenomena such as the double layer effect. In the following section, an implementation has been carried out in order to reproduce the internal double layer effect, which normally leads to a slower response of the electrolyser correcting the false sudden change of the voltage.

A comparison between the chemical-thermal model and an equivalent electrical model is carried out to validate the results and highlight the improved realism obtained with the developed model.

In the end, an additional implementation has been conducted in order to simulate the crossover effect of both hydrogen and oxygen through the membrane.

5.1 Water content

The previous approach doesn't consider the possibility to differentiate between the liquid and the vapor phase of water at the outlet of the anode and cathode. In fact, even if liquid water is introduced in the cell, it is still possible to have a portion of water vapor at the exit and a distinction between liquid and vapor content in the electrode has to be done.

The water balance at the anode can be expressed in the following way:

$$\frac{dN_{\rm H_2O,an}}{dt} = \dot{N}_{\rm H_2O,in} - \dot{N}_{\rm H_2O,mem} - \dot{N}_{\rm H_2O,an~out} = \dot{N}_{\rm H_2O,in} - \dot{N}_{\rm H_2O,mem} - \left(\dot{N}_{\rm H_2O,an~out}^{\rm liq} + \dot{N}_{\rm H_2O,an~out}^{\rm vap}\right)$$
(64)

The water content at the anode itself is then partially made of liquid and vapour phase:

$$N_{\rm H_2O,an(t)} = N_{\rm H_2O,an(t)}^{\rm liq} + N_{\rm H_2O,an(t)}^{\rm vap}$$
 (65)

To distinguish between the two it is necessary to consider the saturation pressure at the working temperature of the electrolyser. The maximum amount of vapour content that can be present at the anode is calculated through the equation of the ideal gas in the following way:

$$N_{\rm H_2O,an}^{\rm vap,max}(t) = \frac{P_{\rm sat} \cdot V_{\rm an}}{R_u \cdot T}$$
(66)

page 40 Master Thesis

From this, considering $N_{\rm H_2O,an}(t)$, if the calculated moles are higher than the one corresponding to the saturation pressure at the same T, then both liquid and vapor content are present in the anode; instead, if the amount is less, only the vapor phase is present and with a pressure lower than the saturation one. In the first case, the amount of vapor will be limited to the one corresponding to the equation of the ideal gas law with $P_{\rm sat}$ and T, while the rest of the moles will be of liquid water at a higher pressure than the saturation one.

To sum up:

Case A – Both liquid and vapor:

$$N_{\rm H_2O,an}(t) \ge N_{\rm H_2O,an}^{\rm vap,max} \Rightarrow \begin{cases} N_{\rm H_2O,an}^{\rm vap}(t) = N_{\rm H_2O,an}^{\rm vap,max} \\ N_{\rm H_2O,an}^{\rm liq}(t) = N_{\rm H_2O,an}(t) - N_{\rm H_2O,an}^{\rm vap,max} \\ P_{\rm H_2O,an}^{\rm vap} = P_{\rm sat}(T) \end{cases}$$
(67)

At the same T of the cell. The liquid water is at the pressure of the anode.

Case B – Only vapor phase:

$$N_{\rm H_2O,an}(t) < N_{\rm H_2O,an}^{\rm vap, max} \Rightarrow \begin{cases} N_{\rm H_2O,an}^{\rm vap}(t) = N_{\rm H_2O,an}(t) \\ N_{\rm H_2O,an}^{\rm liq} = 0 \\ P_{\rm H_2O}^{\rm vap} = \frac{N_{\rm H_2O,an}^{\rm vap} \cdot R_u \cdot T}{V_{\rm an}} \end{cases}$$
(68)

Similarly, the output moles can be both in the liquid and vapor phase:

$$\dot{N}_{\rm an}^{\rm out} = \dot{N}_{\rm O_2}^{\rm out} + \dot{N}_{\rm H_2O,an}^{\rm out} = \dot{N}_{\rm O_2}^{\rm out} + \dot{N}_{\rm H_2O,an,out}^{\rm vap,out} + \dot{N}_{\rm H_2O,an}^{\rm liq,out} = \dot{N}_{\rm an}^{\rm gas} + \dot{N}_{\rm H_2O,an}^{\rm liq,out}$$
(69)

From the moles of liquid water at the anode, the amount of liquid water exiting the anode can be considered as a percentage of the total liquid content:

$$\dot{N}_{\rm H_2O,an}^{\rm liq,out} = k \cdot N_{\rm H_2O,an}^{\rm liq} \tag{70}$$

with k being the liquid water removal coefficient in [1/s]. Depending on the value of k, it is possible to have a fast or slow removal of water from the anode compartment. The higher k is, with an instantaneous draining ideally reached at k=1, the faster the exiting of liquid water from the cell. Instead, the lower k is the greater the accumulation of water at the electrode. The value of k has been hypotized for the simulation and a value of k=0.8 has been considered.

From that, still calculating the output moles as before, which refers to gasses exiting, we can write:

$$\dot{N}_{\rm gas,an}^{\rm out} = \dot{N}_{\rm O_2}^{\rm out} + \dot{N}_{\rm H_2O,an_out}^{\rm vap} = k_{\rm ao} \cdot (P_{\rm an} - P_{\rm el}) \qquad [mol/s]$$

$$(71)$$

still with:

$$P_{\rm an} = P_{\rm O_2} + P_{\rm H_2O}^{\rm vap} \tag{72}$$

and the partial pressure of the oxygen calculated as seen before in Equation 11.

Then, we proceed similarly to before:

$$\dot{N}_{\rm O_2}^{\rm out} = y_{\rm O_2} \cdot \dot{N}_{\rm gas,an}^{\rm out} \tag{73}$$

$$\dot{N}_{\mathrm{O}_{2}}^{\mathrm{out}} = y_{\mathrm{O}_{2}} \cdot \dot{N}_{\mathrm{gas,an}}^{\mathrm{out}}$$

$$\dot{N}_{\mathrm{H}_{2}\mathrm{O,an_{o}ut}}^{\mathrm{vap}} = y_{\mathrm{H}_{2}\mathrm{O}}^{\mathrm{vap}} \cdot \dot{N}_{\mathrm{gas,an}}^{\mathrm{out}}$$

$$(73)$$

From this consideration, we take into account that a part of liquid and vapor content of water can still be present inside the anode, with a part of it (the major content) exiting the electrode.

The same is done for the cathode side:

$$\frac{dN_{\rm H_2O,ca}}{dt} = N_{\rm H_2O,mem} - N_{\rm H_2O,ca,out} = N_{\rm H_2O,mem} - \left(N_{\rm H_2O,ca,out}^{\rm vap} + N_{\rm H_2O,ca,out}^{\rm liq}\right)$$
(75)

With:

$$N_{\rm H_2O,ca(t)} = N_{\rm H_2O,ca(t)}^{\rm liq} + N_{\rm H_2O,ca(t)}^{\rm vap}$$
 (76)

Similarly, liquid water and vapor water can be both found in the cathode and at the output. Same considerations are done regarding the moles of gas exiting and the same equations are used for calculating the number of water vapor and outlet hydrogen.

From these considerations, variations in the thermal block have also to be considered.

The following modification is introduced for the thermal behavior of the electrolyser, including adjustments related to the output molar flows:

$$\frac{dE}{dt} = \dot{Q}_{\text{gen}} - \dot{Q}_{\text{loss}} - \dot{Q}_{\text{cool}} + \sum_{i} \left(\dot{m}_{i}^{\text{in}} \cdot h_{i}^{\text{in}} \right)
- \left[\dot{m}_{\text{H}_{2}\text{O,liq}}^{\text{out}} \cdot h_{\text{H}_{2}\text{O}}^{\text{liq}}(T) + \dot{m}_{\text{H}_{2}\text{O,vap}}^{\text{out}} \cdot \left(h_{\text{H}_{2}\text{O}}^{\text{liq}}(T) + \Delta h_{\text{vap}}(T) \right)
+ \dot{m}_{\text{H}_{2}}^{\text{out}} \cdot h_{\text{H}_{2}}^{\text{out}}(T) + \dot{m}_{\text{O}_{2}}^{\text{out}} \cdot h_{\text{O}_{2}}^{\text{out}}(T) \right]$$
(77)

A difference between the liquid and vapor exiting flows is introduced. The $\Delta h_{\rm vap}(T)$ depends on the working temperature of the electrolyser, which for this tractation is considered around 80°C. Furthermore, it is important to note that the passive cooling effect is carried by the input water, so still conducted by the water in liquid phase.

Dynamic activation overvoltage 5.2

The previously described model can replicate a correct behavior of an electrolyser when it comes to a constant input of current, but it presents some limitations with a fast change in terms of input signal. In particular, it is important to consider that the activation overvoltage cannot instantly vary from one value to another. To consider this transient passage with a dynamic input, the double layer effect has been considered in the model.

The double layer effect consist in the accumulation of charges between the electrode and the electrolyte on both sides of the membrane, resulting in a capacitive effect during the working operation of the electrolyser. Consequently, it causes a time delay with a slow response with respect to a variation of the input signal of current.

page 42 Master Thesis

Modelling this effect allows to reproduce a real behaviour of the component with respect to a dynamic input signal [27]. To consider the described phenomena, this implementation for the activation overvoltage has been considered:

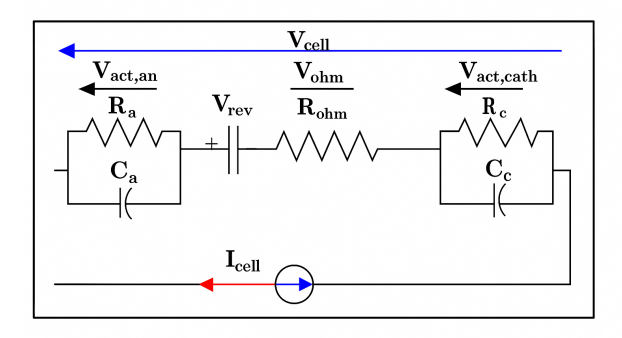


Figure 17: Double layer representation in an equivalent electrical circuit

It is possible to express the voltage of the electrolyser in the following way:

$$V_{\text{cell}} = V_{\text{rev}} + V_{\text{act,an}} + V_{\text{act,cat}} + V_{\text{ohm}}$$
(78)

with:

$$\frac{dV_{\text{act,an}}}{dt} = \frac{1}{C_a} I_{\text{cell}} - \frac{1}{\tau_a} V_{\text{act,an}}$$

$$\frac{dV_{\text{act,cath}}}{dt} = \frac{1}{C_c} I_{\text{cell}} - \frac{1}{\tau_c} V_{\text{act,cath}}$$
(79)

- *C*: represents the double-layer capacitance, defined for both the anode and the cathode [F]
- $\tau = R \cdot C$: is the time constant [s] of the dynamics, where R_{eq} is the equivalent resistance (first for the anode, and similarly for the cathode)

The equivalent capacitance of the electrodes is calculated assuming that the double layer behaves as a parallel plate collector:

$$C = \frac{\varepsilon \cdot A}{d} \tag{80}$$

where:

- $\varepsilon = \varepsilon_r \cdot \varepsilon_0$: dielectric permittivity [F/m], where ε_r is the relative permittivity and ε_0 is the vacuum permittivity.
- A: surface area of the electrode plate (anode or cathode) [m²]
- d: distance between the electrode and the electrolyte. A general value of 1×10^{-9} m is assumed. This value is consistent with the typical thickness of the inner Helmholtz layer

(0.3-0.8 nm) and with the total double-layer thickness (1 nm), which include the Stern and diffuse layers [28].

The calculation of the capacitance is done both for the anode and the cathode, and to simplify the tractation, the same value of capacitance is assumed.

To calculate the time constant, a focus has been done with respect to the resistance. Considering that for $t \to \infty$, i.e. in steady-state conditions, the derivative of the activation voltage tends to zero:

$$\frac{dV_{\text{act}}}{dt} = 0 \tag{81}$$

From the dynamic equation:

$$0 = \frac{I_{\text{cell}}}{C} - \frac{V_{\text{act}}}{\tau} \quad \Rightarrow \quad V_{\text{act}} = \frac{\tau \cdot I_{\text{cell}}}{C}$$
 (82)

Recalling that $\tau = R_{eq} \cdot C$, we obtain:

$$V_{\text{act}} = \frac{R_{\text{eq}} \cdot C}{C} \cdot I_{\text{cell}} \tag{83}$$

With item R_{cell} representing the equivalent resistance of the considered electrode. Since it is already known how to express the active voltage in stationary conditions, as previously seen in Equation 43, then in stationary conditions the two expressions should be the same and from this we can obtain the equivalent resistance:

$$R_{\text{eq}} = \frac{R_u \cdot T}{\alpha \cdot F \cdot I_{\text{cell}}} \cdot \sinh^{-1} \left(\frac{j}{2j_0} \right)$$
 (84)

- R_u : universal gas constant [J/(mol·K)]
- T: temperature of the electrode, assumed to be equal to the cell temperature [K]
- α : charge transfer coefficient [-]
- *j*: current of the cell [A]
- *F*: Faraday constant [C/mol]

Since we are considering stationary conditions for this calculations, the value of the input curret and the target working temperature of the electrolyser are considered as j and T.

In this way, the time constant is calculated as the product of the C and the cell current and $\tau = R_{eq} \cdot C$ is substituted in Equation 79 to obtain the complete expression.

The validation of this implementation has been considered valid taking into considerations the steady state values reached after the transition time similarly to the original validation done in the base model, since it was not possible to verify in particular the specific values obtained from the knee in the curves. Although, since the behavior seems to respond similarly to before, this implementation has been considered accepted.

page 44 Master Thesis

5.3 Results

The results discussed in this section will be obtained considering firstly an ideal response with respect to a constant input current and secondly to a step one. Secondly, a photovoltaic field will be considered as input power for the stack to investigate the response of the stack coupled with renewable energy. The outputs under analysis are the partial pressures of hydrogen and oxygen at the cathode and the anode, the H2 production over time and the voltage behaviour with respect to time.

The considered PEM is made of NAFION 117 and it is Pt anode and cathode based. The specifications of the used electrolyser are present in the figure below and have been used for the analysis. A size of 100 kW has been considered for the stack, and because of that the maximum current accepted for this simulation has been considered in order not to exceed that power size.

Parameter	Description	Value	Unit
n	Number of cells	380	
T_{in}	Temperature of the inlet	25	°C
T_c	Cell temperature	80	°C
A	Electrodes surface	100	cm ²
t_{me}	Membrane thickness	0.0183	cm
P_{ext}	External pressure	101325	Pa
V_{an}, V_{cat}	Electrodes volume	0.001	m^3
k_{ao}	Anode outlet flow coefficient	2.5×10^{-6}	mol/s·Pa
$k_{\rm co}$	Cathode outlet flow coefficient	2×10^{-6}	mol/s·Pa
EW	Equivalent weight of membrane	1100	kg H ₂ O/kg Nafion
d_m	Density of dry membrane	1.78	mol/m ³
$i_{0,an}$	Exchange current density (an-	1E-12	A/cm ²
	ode)		
$i_{0,\mathrm{cat}}$	Exchange current density (cath-	0.001	A/cm ²
	ode)		
α_a	Transfer coefficient (anode)	2	
α_c	Transfer coefficient (cathode)	0.5	
V_{th}	Thermoneutral voltage	1.481	V
$M_{ m H_2O}$	Water molar weight	18.0	kg/kmol
$C_{p,\mathrm{H}_2\mathrm{O}}$	Heat capacity of H ₂ O	75.4	J/mol·K
C_{p,H_2}	Heat capacity of H ₂	28.63	J/g·K
C_{p,O_2}	Heat capacity of O_2	29.248	J/g·K
$C_{p,\mathrm{H}_2\mathrm{O},0}$	Heat capacity of H ₂ O (liquid)	4.18	J/g·K
h_c	Convective heat transfer coeff.	15	W/m ² K
h_r	Radiative heat transfer coeff.	4.5	W/m ² K
A_{ext}	External area	700	cm ²
$T_{ m outside}$	External temperature	25	°C
ε_0	Vacuum permittivity	8.85E-12	F/m
$arepsilon_r$	Relative permittivity	24	
d	Distance between electrode and	1E-9	m
	electrolyte		
λ	Water content	20	
l	Excess of water	15	

Table 2: Model parameters for the PEM electrolyzer

The electrolyser working temperature has been considered equal to 80°C and this value has been reached naturally during the simulation starting from an initial Temperature of 25°C. Instead,

for the working pressure at anode and cathode, no pressure has been imposed but instead they have been reached naturally depending of the outlet flow coefficients considered.

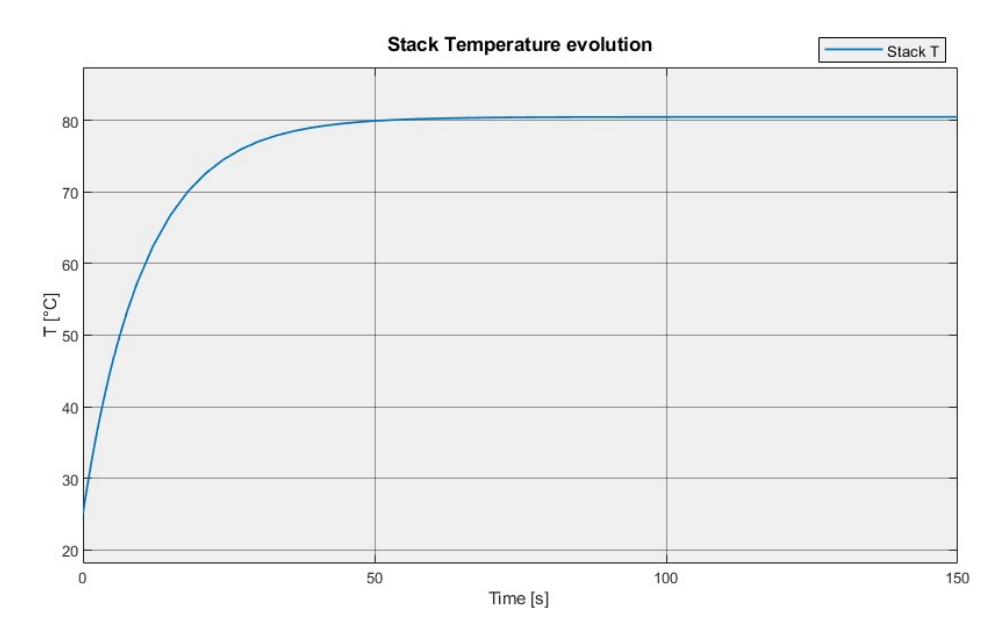


Figure 18: Stack temperature evolution

5.3.1 Constant input current

For the first part, a constant input current with a corresponding value of 100 A has been used and the following voltage response has been obtained. The simulation time is of 150s.

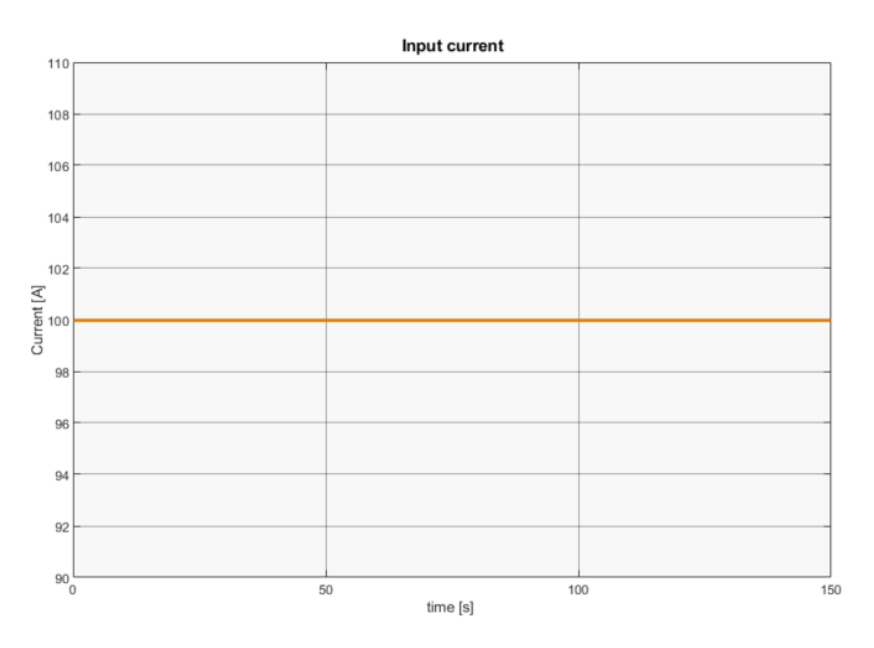


Figure 19: Input current

To initialize the voltage, theoretically at the beginning of the simulations the contributions of

page 46 Master Thesis

the overvoltages should be considered equal to zero and a gradual increase should be observed while the electrolyser starts working and because of that, the initial value of the voltage should be equal to the reversible term expressed in Equation 38.

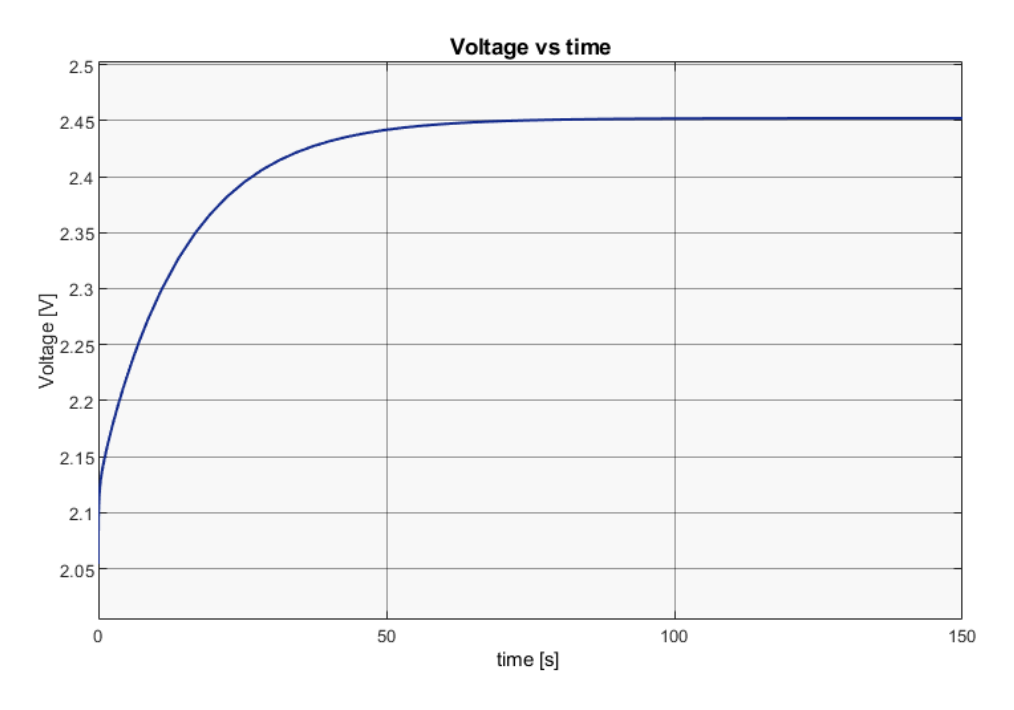


Figure 20: Voltage of a single cell in time

Although, it is possible to see that the starting voltage is a little bit higher than expected, due to the presence of the overvoltages from the start.

In fact, considering a constant input current and considering that both the Activation and Ohmnic overvoltages, Equations 43 and 46, depends on the temperature of the cell, starting from an initial value of 25°C their initial value cannot be considered equal to zero, but an initial contribution is still to be considered. From these considerations, the higher initial value of the electrolyser can be justified. A gradual increase can be seen, as expected, following the increase of the temperature until an asymptotic value around 2.45 V is reached.

To validate the implementations introduced about the phase differences for the water content at the anode and the cathode and the double layer effect, an equivalent electrical circuit has been implemented in the model and the voltage curve of a single cell was used for the comparison.

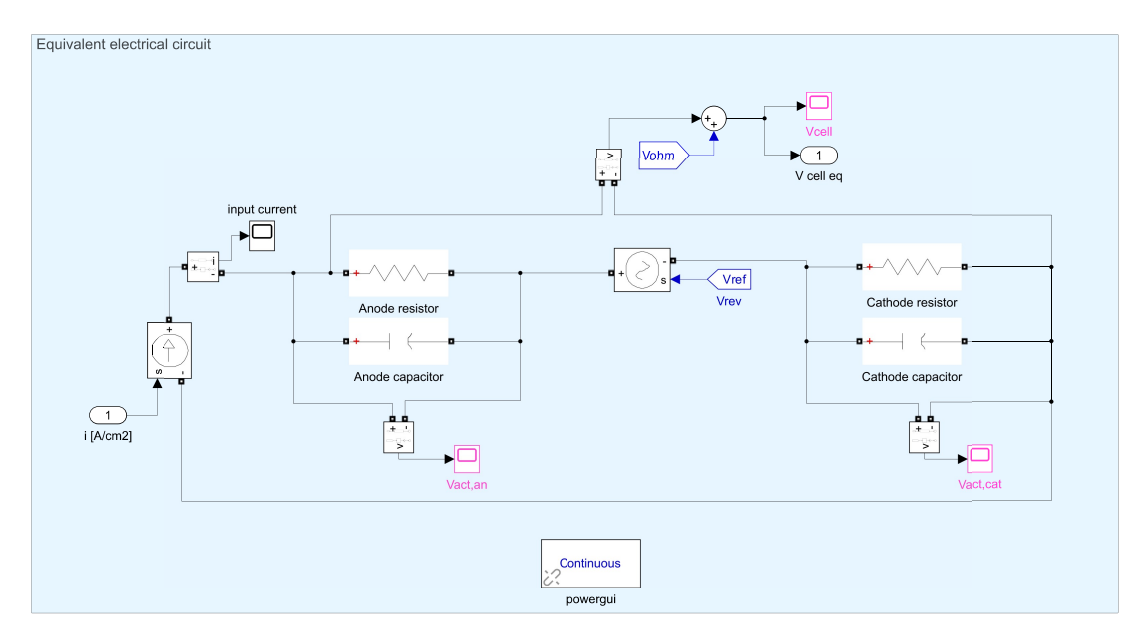


Figure 21: Equivalent electrical circuit

The equivalent circuit is characterized by a current input signal introduced through a controlled current source, and by two parallel connections, in series between them, of a resistor and a capacitor which represent the behavior of the anode and cathode in terms of activation voltage. The capacitor models the charge accumulation associated with the internal double layer effect. The ohmic and resistive overvoltages are included in the model and are calculated separately in the other part of the system. This section specifically focuses on accurately reproducing and analyzing the activation phenomenon and the double layer effect.

Regarding the values used for the resistors and the capacitors, they have been calculated using the flat plate collector formula in Equation 80 and the steady state valued of the resistor calculated in Equation 84.

Side	Resistance	Capacitance
Anode	0.005Ω	0.0021 F
Cathode	$0.00428~\Omega$	0.0021 F

Table 3: Resistance and capacitance values for anode and cathode sides

Below it is possible to see the voltage characteristic obtained from the equivalent model.

page 48 Master Thesis

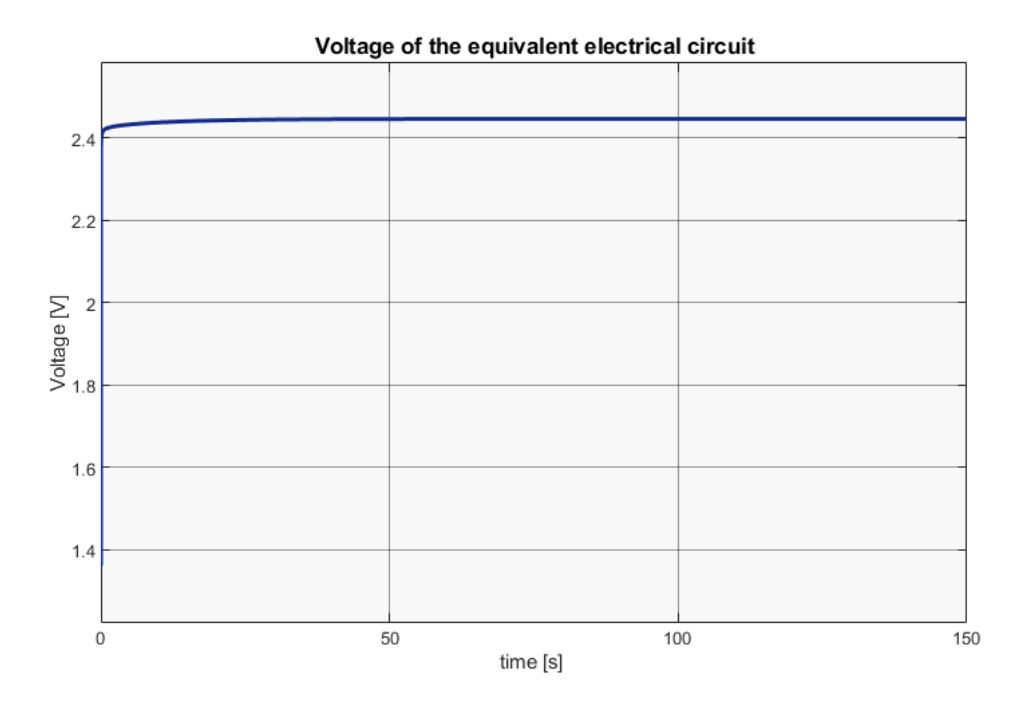


Figure 22: Voltage characteristic in the equivalent electrical circuit

As it is possible to see in Figure 22, the starting voltage is 1.35 V, equal to the reversible voltage, but a fast increase is observed in the very first seconds leading to reaching rapidly the steady state value of 2.45 V. The curve obtained from the equivalent circuit doesn't consider the contribution of the Temperature and its gradual evolution, reason why the characteristic starts from the reversible voltage and a gradual knee cannot be observed, as it is clearly present in the previous voltage curve in which the initial conditions are considered directly at 25°C also for the overvoltages.

With respect to the partial pressures of the components at the anode and cathode side, it is possible to see that the starting pressure at the electrodes is equal to 1 bar, in equilibrium with the external environment. At the anode side, the total pressure is given by the sum of the partial pressure of the oxygen and of the vapor content generated, of which the maximum pressure is equal to the saturation one as already mentioned in the previous chapter. The same considerations but using hydrogen instead of oxygen are made for the cathode.

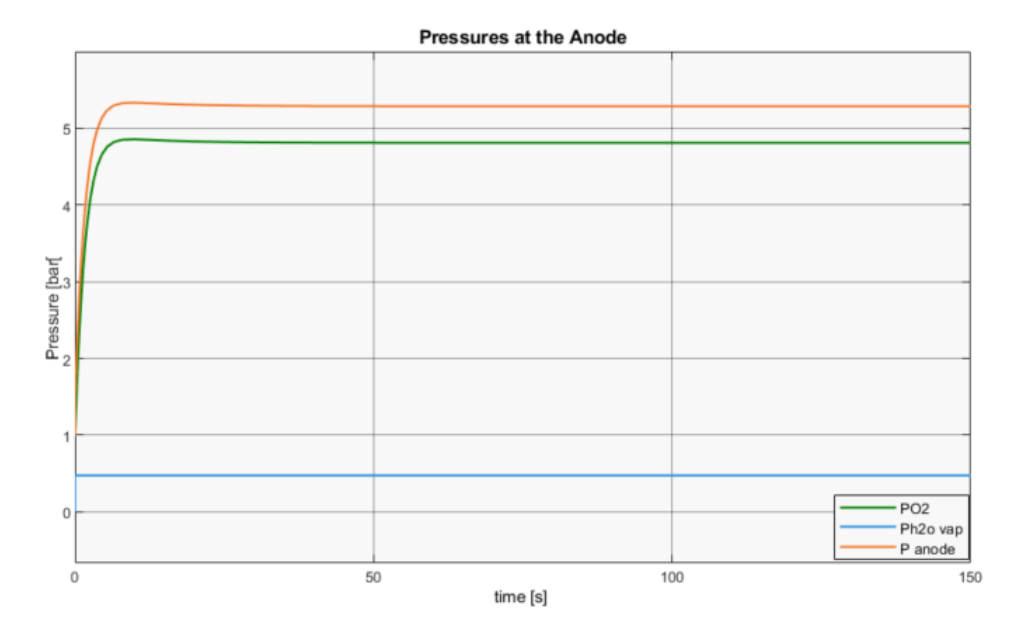


Figure 23: Pressures at the anode

The partial pressure of both the oxygen and the hydrogen at the beginning is equal to the total pressure, since no contribution from the vapor is present yet. Then, almost immediately the vapor content reaches the saturation levels and a pressure of 0.477 bar is obtained. For the oxygen a more gradual increase is reached and the same can be noticed for the total pressure, as the sum of the two. The asymptotic values reached are 4.82 bar for the oxygen and 5.3 bar for the Anode. A higher pressure can be obtained modifying the Anode outlet flow coefficient by decreasing it. Instead, lower values are obtained for the Cathode side.

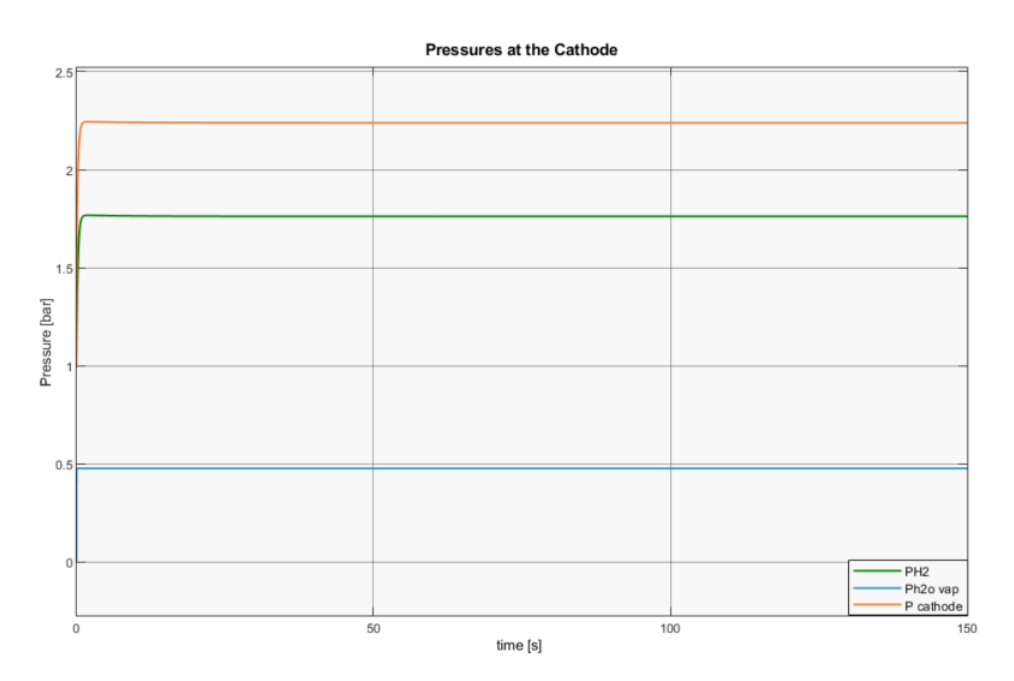


Figure 24: Pressures at the cathode

page 50 Master Thesis

An asymptotic value of 2.3 bar is reached for the Cathode, with a corresponding 1.82 bar for the hydrogen. Its partial pressure is quite low due to the use of a higher cathode outlet coefficient with respect to the anode's one. To obtain higher values of hydrogen's pressure, a lower coefficient must be used.

Regarding the Hydrogen production, it is possible to see a fast increase around the first tens of seconds and then an asymptotic value below 0.2 mol/s. The hydrogen production is constant during the operation of the electrolyser due to the constant input current.

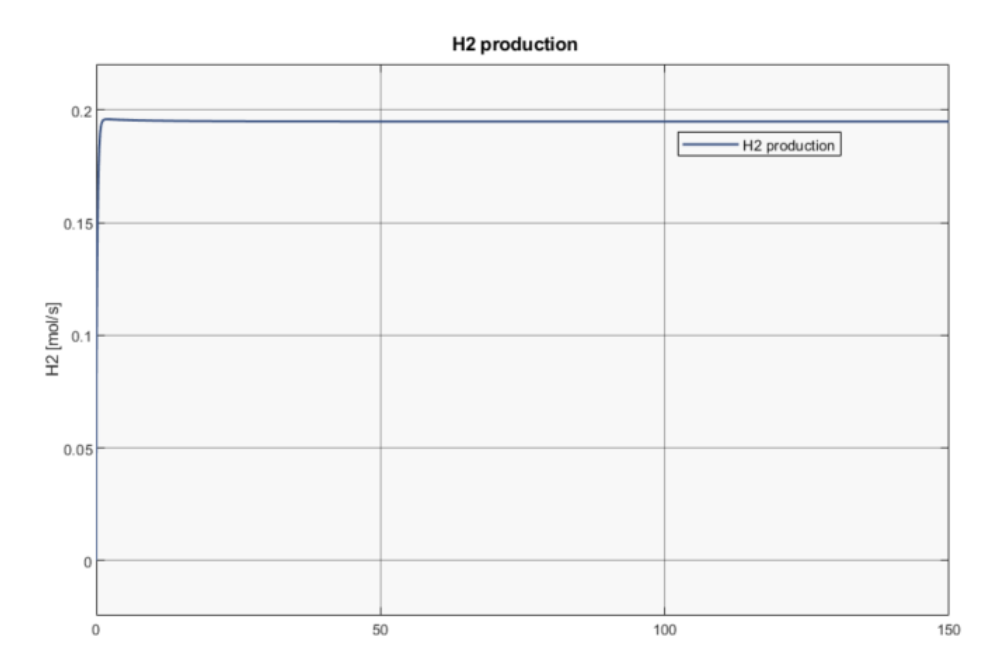


Figure 25: H2 production

5.3.2 Step input current

In a second analysis, a variable step input current shown in Figure 26 has been considered to see the difference of response of the PEM in terms of pressures, voltage and hydrogen production. The main goal of this analysis was to enhance the implementation obtained with respect to the voltage.

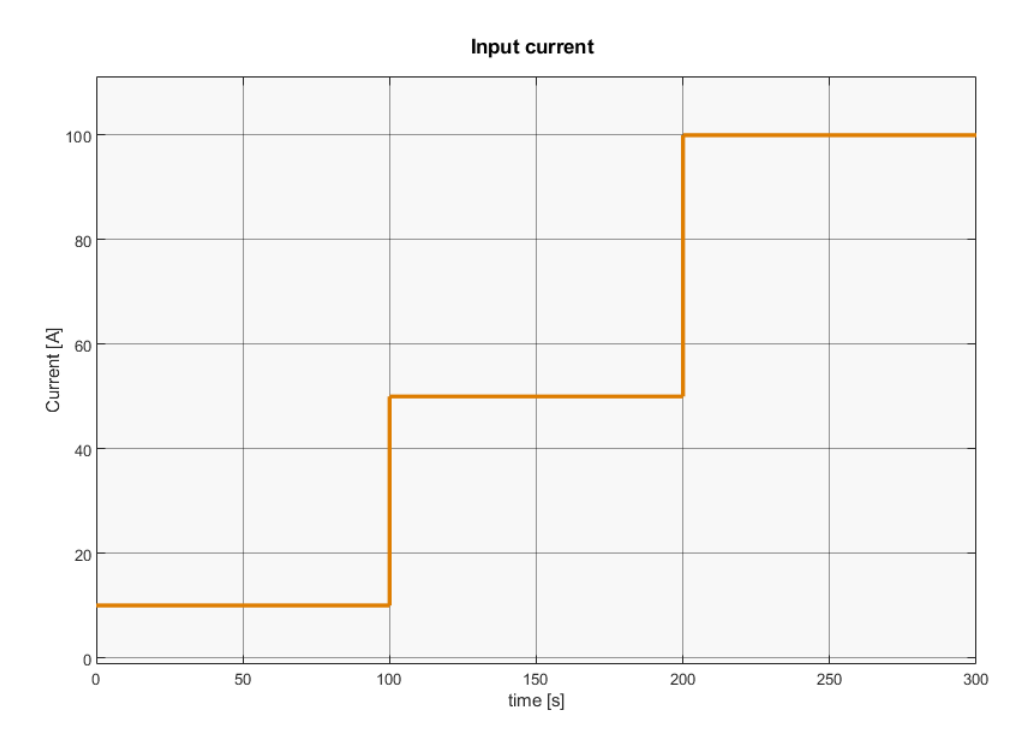


Figure 26: Variable input current

All of them tend to reproduce the characteristics they had in the previous analysis and tend to increase as the input current increases, but following the change of magnitude of the current still with a knee and then a steady-state value.

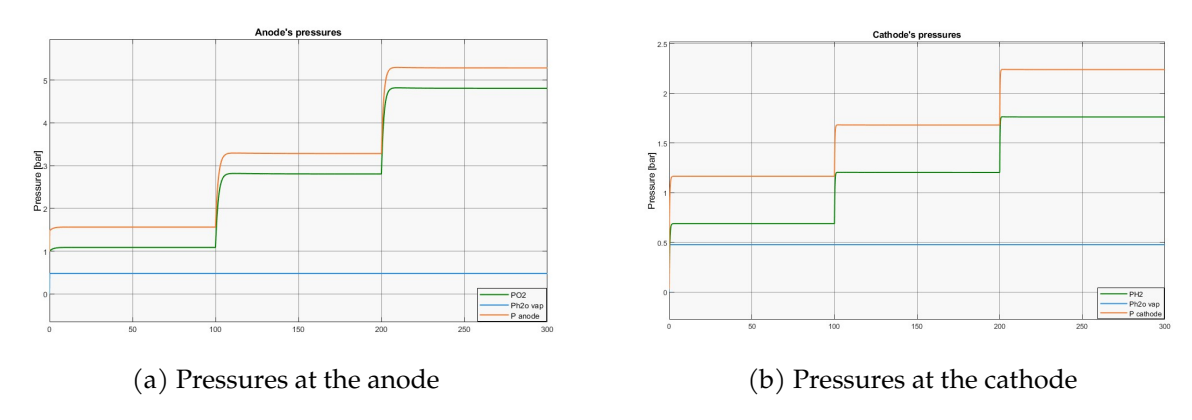


Figure 27: Pressures at the electrodes.

The implementations introduced the main difference compared to the reference electrical model. In the latter, the transient evolution of the voltage during the changes of amplitude shows a small knee due to the double layer effect represented by the presence of the capacitances, but it is not well defined and a faster change is present. In reality, a slower change is despicable due to thermal dynamics adjustments with changes in heat generations and cooling effect of the cell, to electrochemical reaction kinetics with OER and HER adapting to new current and also to water transport through the membrane and oxygen and hydrogen outputs.

page 52 Master Thesis

The current model takes into account these variations and a more explicit transient is visible during the changes. The values reached during the simulations in both the model were pretty much the same, which is useful to show the valiation of the chemical one, but with a main difference in terms of curves evolution.

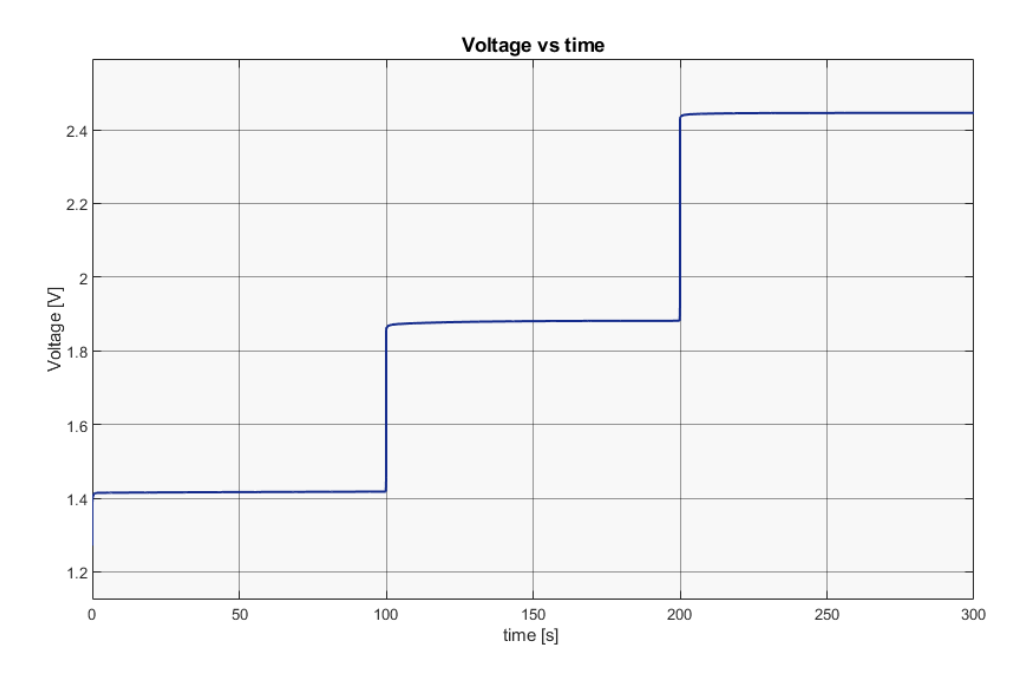


Figure 28: Voltage of a single cell in the electrical model

By a comparison of the two characteristics it is possible to see how during the first input current of $10~\rm A$ the starting value of the electrical one is equal to $1.415~\rm V$ and this value is kept for the whole durations of $100~\rm s$. When a current variation is introduced, reaching $50~\rm A$, a rapid increase up to $1.86~\rm V$ is obtained. From that, during these other $100~\rm s$ it is kept almost constant increasing only up to $1.88~\rm V$. Then, again, after a change up to $100~\rm A$ the voltage has a fast increase up to $2.43~\rm V$ and then a steady state of $2.45~\rm V$.

This behavior does not accurately reflect the variations observed in a real electrolyzer.

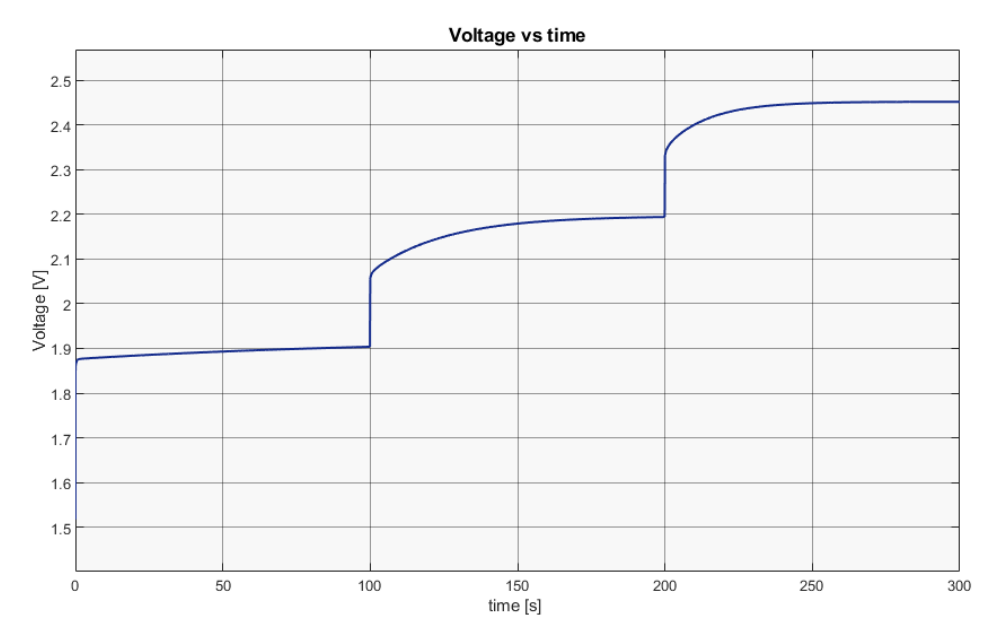


Figure 29: Voltage of a single cell in the chemical model

In the chemical model, the starting voltage is still 1.41 V, but a sudden increase brings it to 1.86 V. This occurs because the overvoltages in the electrolyzer were initialized as zero at the starting time, while in reality both ohmic and activation overvoltage already have small values due to their dependence on temperature. The voltage then gradually increases to around 1.9 V, which is close to the value reached by the electrical model after the first time interval.

When the input current changes, a smaller and fast voltage rise is observed, followed by a slower increase, mainly driven by thermal dynamics. The transition from 10 A to 50 A causes a significant heat generation in the cell, contributing to a slower initial adjustment. The voltage eventually reaches 2.2 V, and during the final current change and time interval, it rises more gradually from 2.34 V to 2.45 V.

The steady-state value reached in this last phase matches the one obtained in the electrical model. However, in this case, the transient evolution more realistically reflects the actual behavior of the electrolyzer.

In the end, the following hydrogen production is obtained.

page 54 Master Thesis

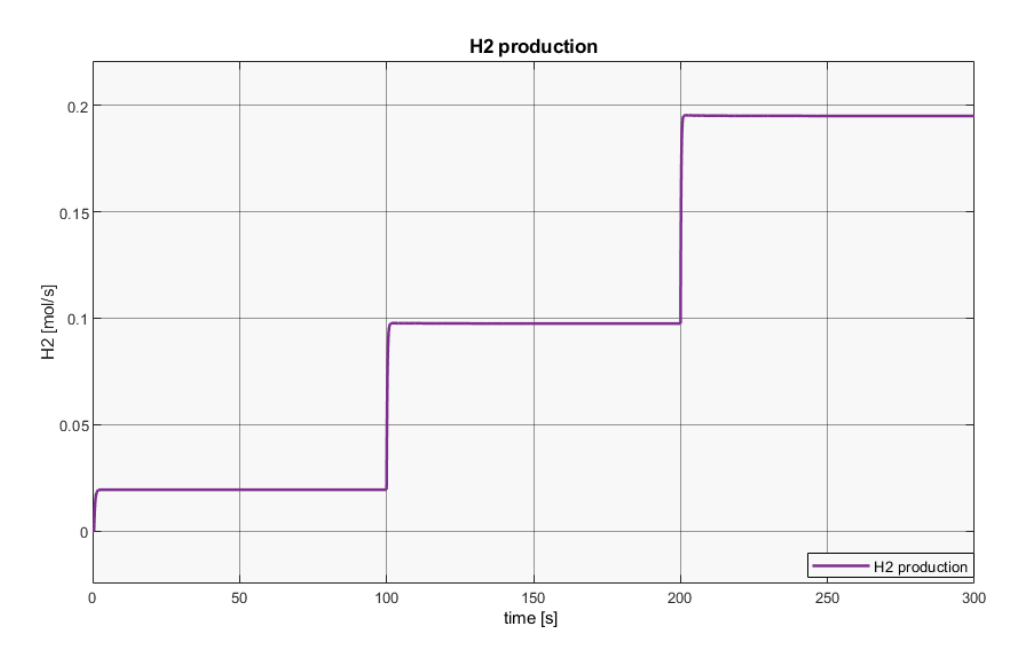


Figure 30: H2 production with a variable current input

It is possible to see how the thermal dynamics mainly affect the voltage characteristic, while the H2 production in mol/s similarly follows the behaviour of the input current with so significant transition delay.

5.3.3 PV input power

For a more realistic analysis, a new power input from a photovoltaic plant was introduced to analyze the behavior of the electrolyser and its hydrogen production with respect to a daily changing input current. The sampling time considered switched to an entire day of 8600 s and all the power produced by the PVs has been entirely sent to the electrolyser. Because of this, the plant has been modeled considering, as previously mentioned, a stack of 100 kW and the same working conditions as before have been considered, both in terms of geometry and maximum working temperature of 80°C.

The data reported below refers to a single photovoltaic panel. Furthermore, the irradiance values have been extracted through the PVGIS software considering June as the reference month and Barcelona, Spain, as the city.

Parameter	Description	Value	
_	Slope	45°	
η	Efficiency	0.23	
A_{pv}	Surface	1.7922 m^2	
\bar{l}	System Losses	14%	
_	Material	Crystalline Silicon	

Table 4: PV Data

Starting from the irradiance, to obtain the solar power the following equations have been used:

$$P = \operatorname{Irr} \cdot A_{\operatorname{pv}} \cdot \eta \qquad [W] \tag{85}$$

The calculated power is then multiplied by a number n in order to consider a total photovoltaic field capable of producing a maximum input power of 100 kW, equal to the stack's capacity. The optimum field size is then equal to 501.81 m2.

Considering that current is used as input for the model, the power has been divided by the voltage of the stack. In Figure 31 it is possible to see both the solar power and the input current curves during the day. The production starts after 5 AM and reaches the maximum at midday, with a slow decrease in the afternoon and then a stops around 6 PM.

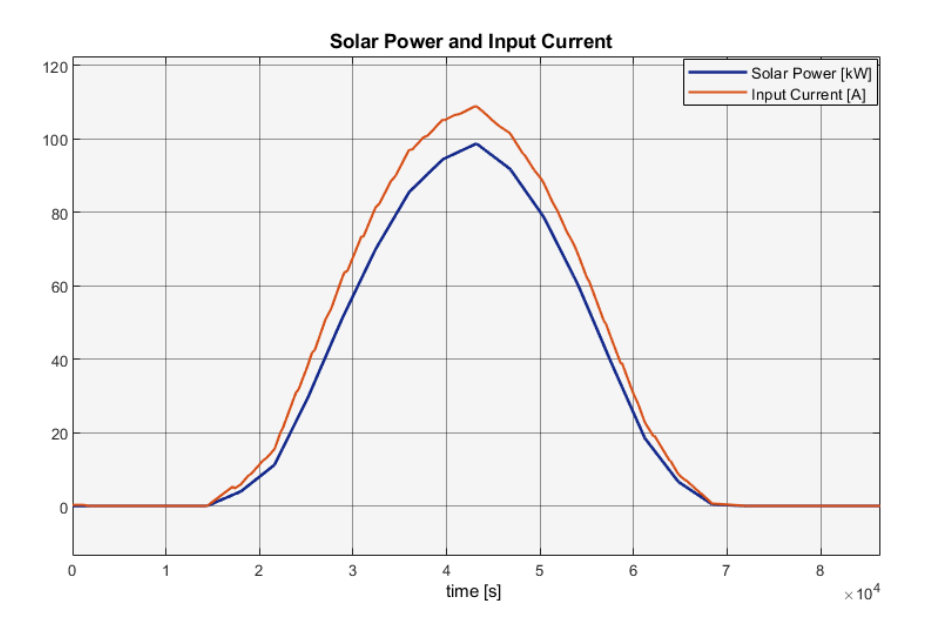


Figure 31: Input power and current

All the previously analyzed parameters, such as the cell voltage, the anode and cathode's partial pressures and the hydrogen production show the same curve behavior as the input current.

page 56 Master Thesis

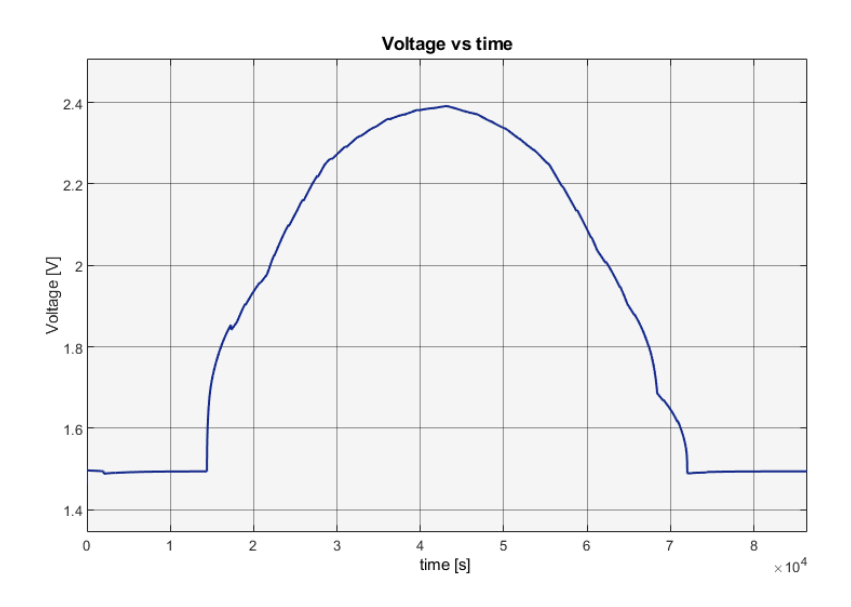


Figure 32: Voltage of a single cell in time

The cell voltage increases from early morning until midday, then decreases in the afternoon until evening. The maximum value reached is 2.4 V, corresponding to a current higher than 100 A. In the previous analysis, for a current of 100 A, the voltage exceeded 2.4 V because the current was kept constant for a longer period, allowing the voltage to rise until a steady state value reached after the transient.

In the present case, due to the dynamic variations of the input current caused by weather conditions and solar exposure, the transient is shorter and subject to rapid changes, preventing the voltage from stabilizing at a constant steady state value.

Instead, the peaks of the anode and cathode pressures are higher than the average values reached before, still due to the less stability introduced by the changing renewable energy.

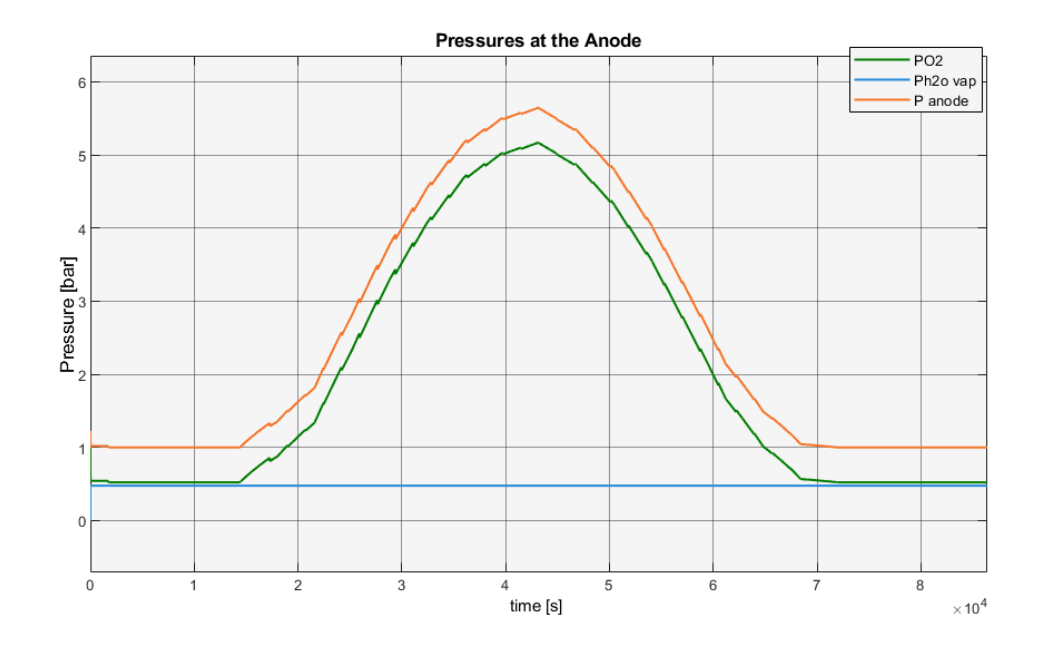


Figure 33: Pressures at the anode

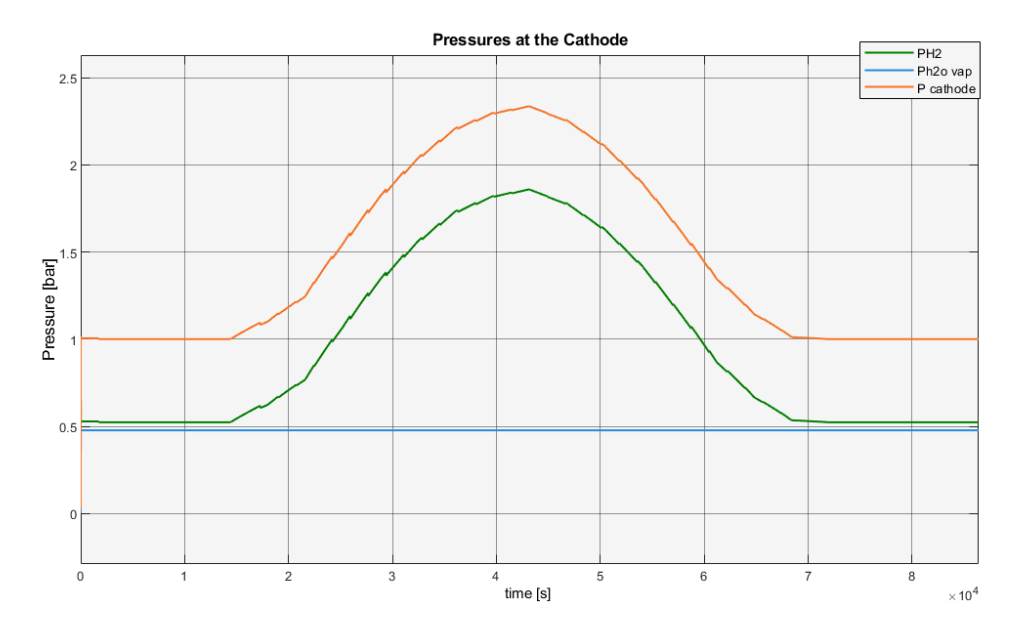


Figure 34: Pressures at the cathode

It is possible to see how the maximum hydrogen production is reached around midday, with a peak of more or less 0.221 mol/s, a little bit higher with respect to the previous analysis due to the higher current reached at midday. With this working conditions, about 12.03 kg of hydrogen and 9.607 of oxygen can be produced per day.

page 58 Master Thesis

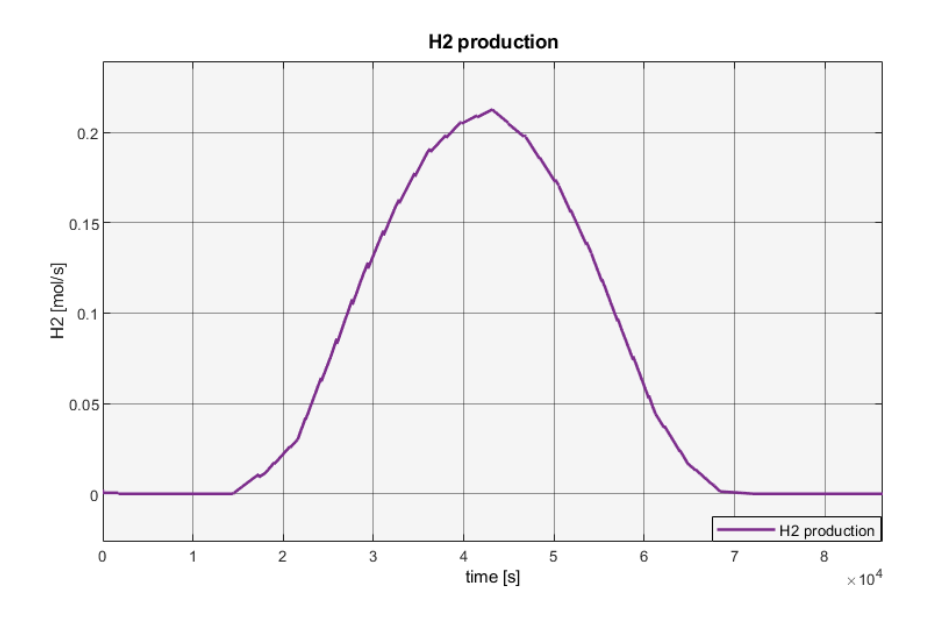


Figure 35: H2 production with a solar power input

It is possible to conduct an analysis to see the effects that the photovoltaic size has on the hydrogen production rate. In Figure 36 a comparison between different PV field sizes and consequently kilograms of hydrogen produced in a day are represented.

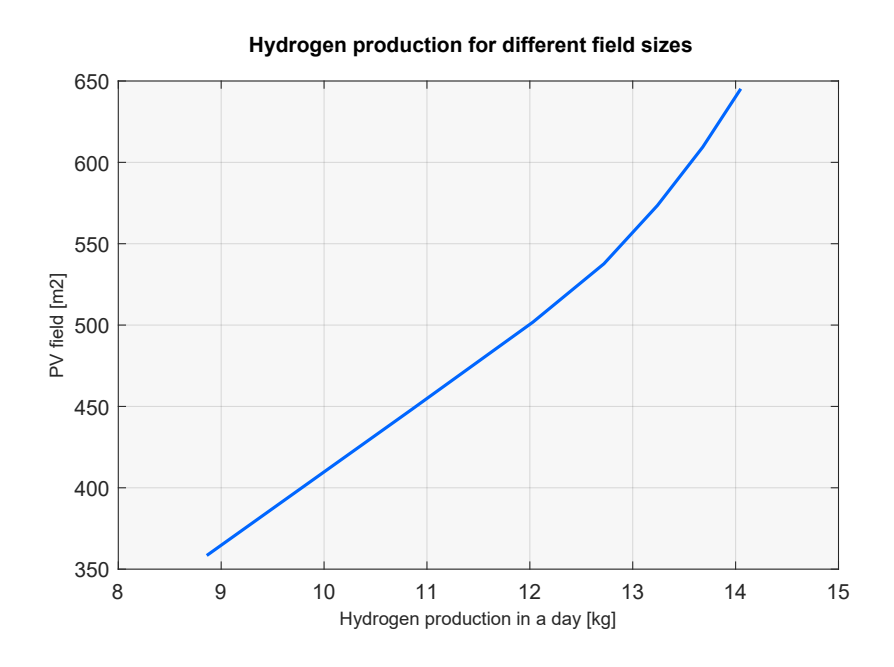


Figure 36: Sensitivity analysis for photovoltaic field

The PV size that produces a power equal to the electrolyser capacity, 501.81 m2, can be considered as the optimum one since for lower values an underutilization of the device is obtained

and for higher values the need for a storage is introduced. For dimensions lower than that, the hydrogen output increases almost linearly until the optimum value of 501.81 m2 is reached. After it, for a higher increase of the field, there's a slower increase of hydrogen production leading to a curvature and a faster growing behaviour of the curve.

For values lower than the optimum field size the maximum rated power is not reached meaning that the stack is underutilized with respect to its capacity. If a smaller size for the photovoltaic field is chosen, the additional required power could be taken from the grid, integrating eventually the electrolyser into grid regulation processes needed for restore the equilibrium in the event of fluctuations caused by renewable sources.

For higher sizes with respect to the optimum one, higher input currents will be reached during earlier hours of the day and the hydrogen production will reach higher values even before midday. In order to respect the size of the electrolyser and to not exceed 100 kW, once the input current becomes too high for its size the additional produced power overcoming the limit should be stored in a battery and then reused in the afternoon/evening hours of the day to compensate for the lower production, reaching a more stable and constant behavior during the whole day. Nevertheless, for the graph it is possible to see that an overdimensioning approach doesn't lead to a greater return, but to a diminishing one instead.

Furthermore, even if not directly investigated, the associated costs to the greater size would not be compensated by the small marginal gains in hydrogen production, leading to the conclusion that overdimensioning the PV field is not the right choice, unless it is coupled to storage batteries eventually re used in a second moment.

6 Part II: Modeling hydrogen and oxygen crossover

6.1 Degradation consequence: Hydrogen and Oxygen crossover

The normal state of working of a PEM electrolyser consists in the transport of H+ ions from the anode to the cathode side, with the formation of H2 at the latter electrode and the "expulsion" of the produced gas from the cathode outlet channels. Nevertheless, a small quantity of hydrogen permeates the membrane in the opposite direction, going back to the anode. The same happens to the oxygen produced at the anode, that passes through the membrane and reaches the cathode side. This phenomenon takes the name of hydrogen and oxygen crossover and has several consequences in terms of reduction of Faraday efficiency, membrane degradation and risk of explosion due to hydrogen's lower level of flammability in air being equal to 4%. Hydrogen crossover is estimated to be twice as much as the oxygen one, therefore only the H2 permeation will be developed in the following chapter [29].

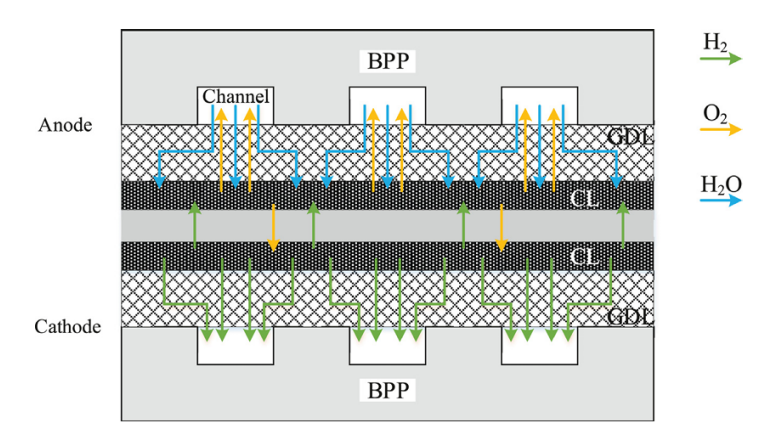


Figure 37: Hydrogen and Oxygen crossover scheme [29]

As previously mentioned in the third chapter, a small percentage of crossover naturally happens in the normal working conditions of the electrolyser, but degradation phenomena may increase the rating. Hydrogen crossover is affected by the increase of temperature and decrease of thickness of the membrane, by hydrogen pressure enhancement on the MEA and by the compression of the gas diffusion layers. The thinning of the membrane decreases the separation path between the anode and the cathode easing the gasses permeation, same as the presence of hot spots that could cause micro cracks on the membrane's surface offering a new path of permeation. Hydrogen's pressure on the membrane also affects the crossover, "pushing" the H2 molecules through it. The low pressures obtained from usual working conditions do not contribute in particular to the permeation, but an eventual compression of gas diffusion layer due to reduction in its thickness and porosity, as mentioned in [29], could contribute to its increase.

Given the limited availability of equations in the literature and the impossibility to obtain specific chemical parameters without direct measurements, the reproduction of the previously mentioned degradation phenomena becomes extremely difficult.

In this section, the gasses crossover under normal working conditions has been investigated and additional equations to the previously developed model have been introduced in order to re-

page 62 Master Thesis

produce the internal phenomena. The amount of hydrogen content at the anode was calculated considering the effect of current density and working temperature changes.

For the modeling, the main references were a section of the article "Energy Conversion and Management: X", a section of the forum "Applied Energy" and a section of the journal "International Journal of Hydrogen Energy", [24] [30] [31].

In general, it is possible to explicit the variation of the mass flows in the cell in the following way:

Equation 9 is modified adding the terms related to oxygen permeation through the membrane, similarly to Equation 19 with hydrogen permeation. The water balance at the anode and at the cathode previously described in Equations 64 and 75 are the same and two additional equations, one for the anode and one for the cathode, are introduced. These account for the presence of hydrogen at the anode and oxygen at the cathode.

Theoretically, the two permeate the membrane through similar mechanisms as water, and it is possible to consider the amount of hydrogen and oxygen permeating the membrane in the following way:

$$\dot{N}_{\rm H_2}^{\rm mem} = \dot{N}_{\rm H_2}^{\rm diff} - \dot{N}_{\rm H_2}^{\rm eo} + \dot{N}_{\rm H_2}^{\Delta P}
\dot{N}_{\rm O_2}^{\rm mem} = \dot{N}_{\rm O_2}^{\rm diff} + \dot{N}_{\rm O_2}^{\rm eo}$$
(87)

The oxygen permeation doesn't consider the term related to pressure difference, since it is more impacting for the hydrogen permeation, while the negative sign of the electro-osmotic component is due to the opposite direction with respect to the other two components. To simplify the analysis, the electro osmotic molar flow is neglected for both the gasses, since the main cause of permeation is due to diffusion phenomena having the electro osmotic one impacting more the water passage through the membrane [31].

As a consequence, in the following formulation we treat two flux densities. The diffusion flux density is obtained through the Fick's law and it depends on the permeability constants, pressure differences of the gas between the anode and the cathode and the membrane thickness. Instead, the flux due to pressure difference, here only defined for the hydrogen, reflects the different pressures between the anodic and cathodic catalyst layer and introduce an additional

driving force and it depends on the permeability coefficient and on pressure difference between the hydrogen at the cathode and oxygen at the anode [24].

Consequently:

$$\dot{n}_{\rm H_2}^{\rm mem} = \varepsilon^{\rm dif} \frac{p_{\rm H_2}^{\rm cat} - p_{\rm H_2}^{\rm an}}{tme} + \varepsilon^{\rm dp} \frac{p_{\rm H_2}^{\rm cat} - p_{\rm O_2}^{\rm an}}{tme} \quad [\text{mol/(s} \cdot \text{cm}^2)]$$
(88)

$$\dot{n}_{\rm O_2}^{\rm mem} = \varepsilon_{\rm O_2}^{\rm dif} \cdot \frac{p_{\rm O_2}^{\rm an}}{tme} \quad [\text{mol/(s} \cdot \text{cm}^2)]$$
(89)

Where:

- $\varepsilon_{\rm H_2}^{\rm dif}$: permeability due to concentration differences between the anode and the cathode $[10^{-11}~{\rm mol/(cm\cdot s\cdot bar)}]$
- $\varepsilon_{\rm H_2}^{\rm dp}$: permeability due to pressure differences $[10^{-11}\,{\rm mol/(cm\cdot s\cdot bar)}]$
- *tme*: membrane thickness [cm]
- $p_{\rm H_2}^{\rm cat}$: partial pressure of hydrogen at the cathode side [bar]
- $p_{\rm H_2}^{\rm an}$: partial pressure of hydrogen at the anode side [bar]
- $p_{O_2}^{an}$: partial pressure of oxygen at the anode side [bar]

The permeability coefficients are dependent on the hydrogen solubility and the diffusion coefficient, which furthermore depends on the working temperature. To simplify the discussion, and due to the lack of elements in the literature, constant values are assumed and constant permeabilities are considered.

The pressures of the oxygen at the anode and hydrogen at the cathode are the same calculated in the previous section. Instead, a simplification is performed on the partial pressure of the hydrogen at the anode side, considering it negligible with respect to the oxygen and water content at the anode [31]. In this way it is possible to neglect it following the same consideration done by Schalenbach et al.

To obtain the constant values, direct measurements on the electrolysers have to be done in order to get the specific fit-in parameters. In theory, starting with initial guessing direct measurements are done on the component and the initially hypothesized constants are adjusted in order to minimize the error between the model and the measurements. Since it was not possible to perform direct measurements on an electrolyzer, the values for these constants are taken from the previously mentioned paper making reference to a PEM electrolyzer using a Nafion N117 as a membrane, with 183 μ m thickness.

The values are reported in the table below. The developed model can be easily adjusted by inserting specific parameters obtained from direct measurements. However, considering that a PEM electrolyzer with the same membrane and working temperature should generally exhibit similar characteristics, values similar to those reported can typically be expected [31].

page 64 Master Thesis

Gas	$\varepsilon^{\mathrm{dif}}$ (10 ⁻¹¹ mol/cm·s·bar)	$\varepsilon^{\mathrm{dp}} \ (10^{-11} \ \mathrm{mol/cm \cdot s \cdot bar})$
H_2	4.65	2
O_2	2	_

Table 5: Fit-in parameters

The final expression of the molar flow of hydrogen and oxygen through the membrane are expressed below:

$$\dot{n}_{\text{mem},H_2} = \varepsilon^{\text{dif}} \frac{p_{\text{H}_2}^{\text{cat}}}{d} + \varepsilon^{\text{dp}} \frac{p_{\text{H}_2}^{\text{cat}} - p_{\text{O}_2}^{\text{an}}}{d} \quad [\text{mol/(s} \cdot \text{cm}^2)]$$
(90)

$$\dot{n}_{\text{mem,O}_2} = \varepsilon_{\text{O}_2}^{\text{dif}} \cdot \frac{p_{\text{O}_2}^{\text{an}}}{d} \quad [\text{mol/(s} \cdot \text{cm}^2)]$$
(91)

To conclude, the amount of hydrogen at the anode side, with respect to the oxygen content, is expressed as:

$$H_2 \text{ in } O_2(\%) = \frac{\dot{n}_{H_2}^{\text{mem}}}{\dot{n}_{H_2}^{\text{mem}} + \dot{n}_{O_2}^{\text{gen}}} \cdot 100$$
(92)

The oxygen content at the cathode side, being usually less considerable with respect to the hydrogen one as previously mentioned, has not been investigated.

The hydrogen percentage with respect to oxygen has been calculated for various input current densities. The dependence on the input current is not immediately visible, but it indirectly affects the hydrogen percentage due to the variations on the pressure that it causes.

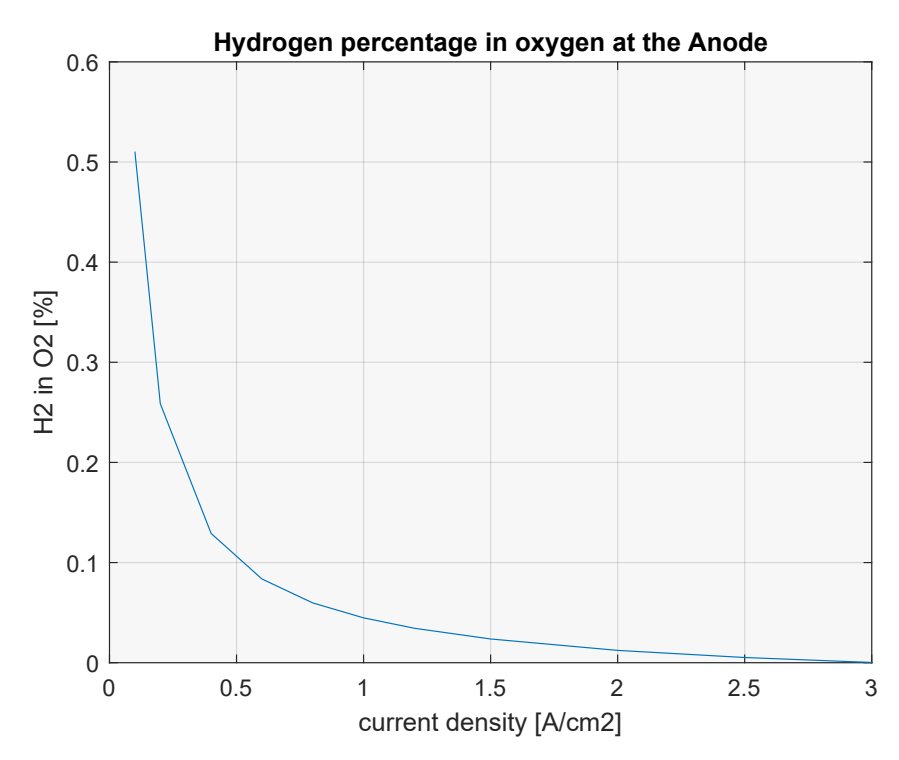


Figure 38: Hydrogen content on the anode side with respect to varying current density

It is important to note that the hydrogen percentage never exceeds the 2% safety threshold typically considered in industrial applications. The values remain notably low primarily due to the membrane thickness and the relatively low pressures on both the anode and cathode sides.

For lower current densities the hydrogen permeation at the anode shows higher values with respect to higher current densities. It can be explained considering that the higher the input current, the higher the oxygen generation and the lower the amount of hydrogen with respect to the total oxygen content. As a consequence, the electrolyser performance and safety conditions tend to be greater with higher power input and higher current densities.

For target temperatures different than 80°C it is possible to see the following behavior:

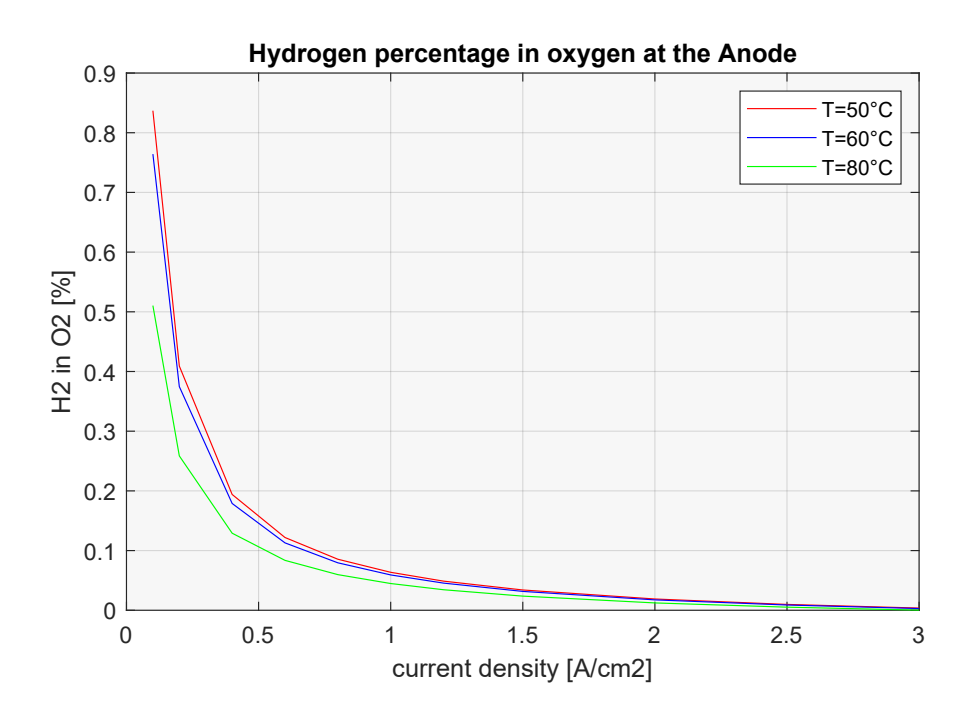


Figure 39: H2 percentage at the anode with different working Temperatures

From this analysis it is possible to see that, the higher the working temperature of the electrolyser, the lower the hydrogen content at the anode for the same input current density.

To understand this behavior it is important to consider that, with an increase of the temperature, the diffusivity of hydrogen increases because the molecules gain more energy and have a higher movement also through the membrane. Then, the first term of the diffusivity contribution in hydrogen crossover increases with the temperature, due to an increase of the permeability coefficient. Although, considering that with an increase of temperature there's an associated increase of the partial pressure of the gasses, as it was seen in Equation 11 with oxygen partial pressure, it is possible to consider an increase both for the hydrogen pressure at the cathode and oxygen pressure at the anode. The higher increase of the oxygen partial pressure, with respect to the hydrogen one, is the reason why the second term in Equation 90 related to the pressure difference decreases. Then, with an increase of temperature, generally the first term increases while the second one decreases. Nevertheless, the decrease of the second one results being

page 66 Master Thesis

higher than the increase of the diffusivity component, leading to a decrease of the hydrogen permeation. Since the number of moles of generated oxygen are the same, not being affected from the change of temperature as outlined in Equation 10, in the calculation of the hydrogen percentage in oxygen at the anode the amount decreases with an increase of temperature. This reasoning is still valid even if constant parameters are assumed for the permeability coefficients, because even if the increase of the diffusivity coefficient with the temperature cannot be represented, the increase of hydrogen partial pressure in the first component is still present. Furthermore, it is validated from the different results and analysis present in the literature, as previously cited.

This difference is more evident for low input current densities, while the curves tend to get closer for higher values to the point that they cannot almost be distinguished.

It is also interesting to note that these kind of electrolysers are able to work safely even with low input current densities, where the hydrogen crossover percentage is higher, resulting in the possibility of using the PEMs for applications that require a flexible modulation and various working operations. They can be easily coupled with a renewable energy technologies, as we have seen in the previous chapter considering the coupling with a photovoltaic field, being able to work with both low and high current densities without encountering significant safety issues.

7 CONCLUSION page 67

7 Conclusion

In this thesis a dynamic realistic model of a PEM electrolyser has been analyzed and simulated through the Matlab/Simulink® environment.

The developed model, which integrates both electrochemical and thermal phenomena, has shown an increase in the degree of realism of the response of the electrolyser, especially with respect to a changing input current as it was seen with a step signal and with the introduction of a photovoltaic module. The introduction of the double-layer capacitance, the differentiation between liquid and vapor phases within the electrodes and the thermal response allowed to reflect the dynamics during a transient response to current variations, reflecting the strict correspondence between chemical-kinetic parameters and electric-thermal ones.

The simulations under photovoltaic input current resulted in the existence of an optimal size for the PV field which ensures the match and the full utilization of the electrolyser capacity. For smaller fields, the stack remains underused and external grid support would be necessary, while an oversizing leads to diminishing returns in hydrogen production and would require additional storage systems to avoid overloading the electrolyser. This underlines the importance of a careful dimensioning of the system, especially in terms of correct energy exploitation and cost management.

Furthermore, the analysis of hydrogen crossover under normal operating conditions confirmed the safety of operation even under low current densities, which usually put the device in a critical operating condition. In the results, the hydrogen content at the anode never exceeded the industrial safety threshold of 2%. In addition, the results also showed that higher operating temperatures and current densities lead to safer and more efficient working conditions, supporting the flexibility of PEM electrolysers in couple with intermittent renewable sources, being able to work both with low and high current densities and to adapt without a significant time delay with respect to a changing input power.

Finally, although the model relies on some constant parameters assumed during the calculations due to the lack of possibility of conducting direct measurements, these can be easily replaced once direct measurements from a real electrolyser are available. The model provides a valuable tool for comparison and prediction, offering a useful insight on the possible future behaviour of a PEM electrolyser under varying operating conditions.

8 Simulink model blocks

8.1 Anode

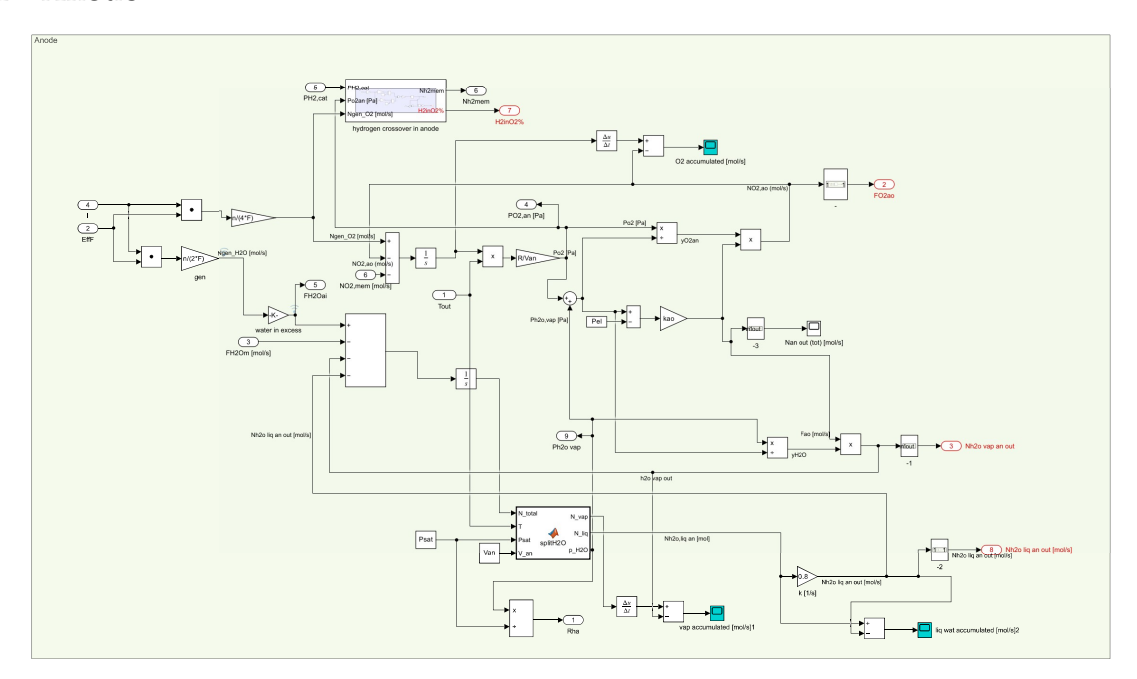


Figure 40: Anode scheme and blocks

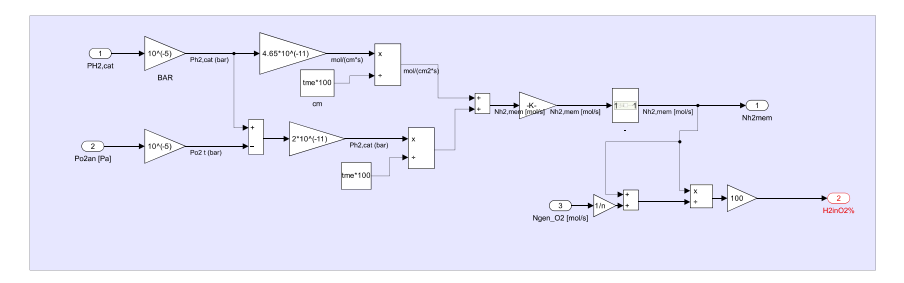


Figure 41: Hydrogen percentage in Oxygen scheme and blocks

page 70 Master Thesis

8.2 Cathode

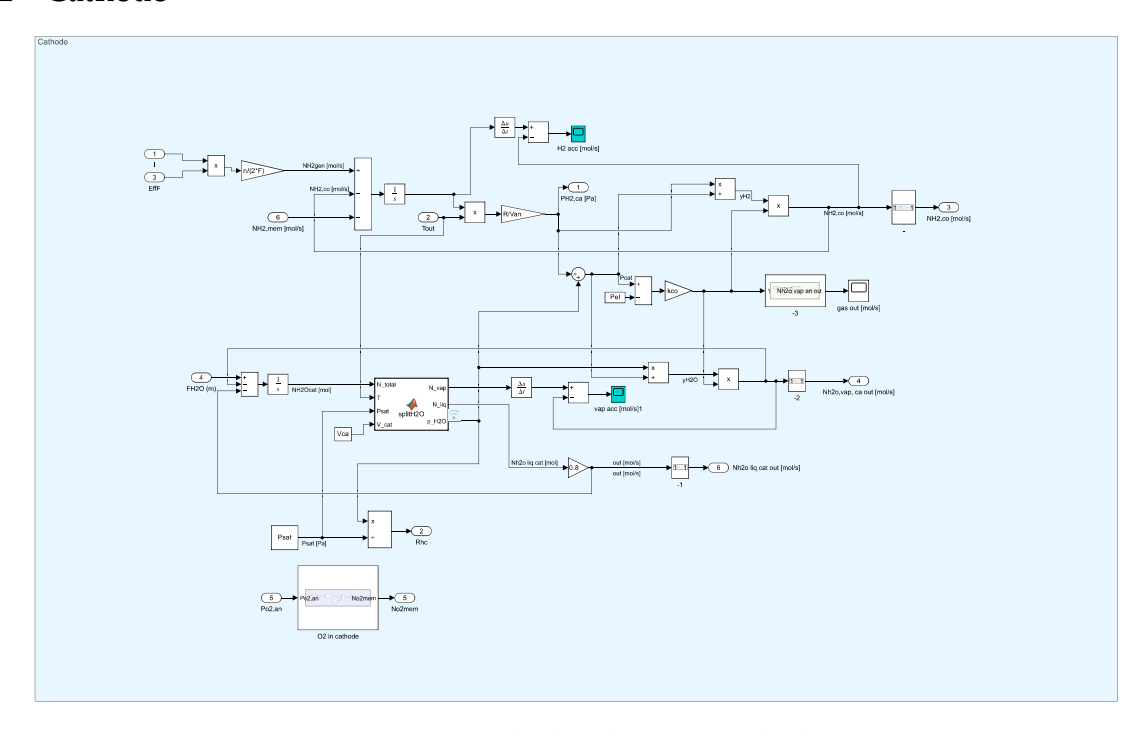


Figure 42: Cathode scheme and blocks

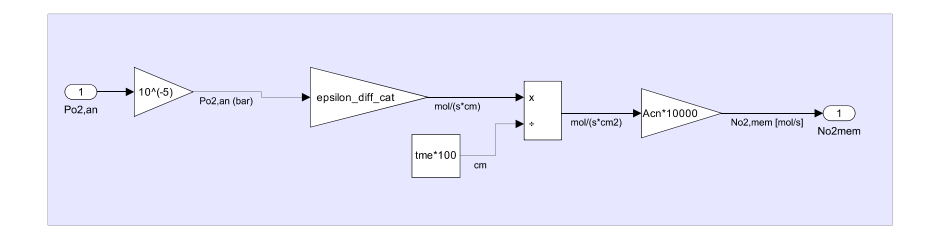


Figure 43: Oxygen crossover scheme and blocks

8.3 Membrane

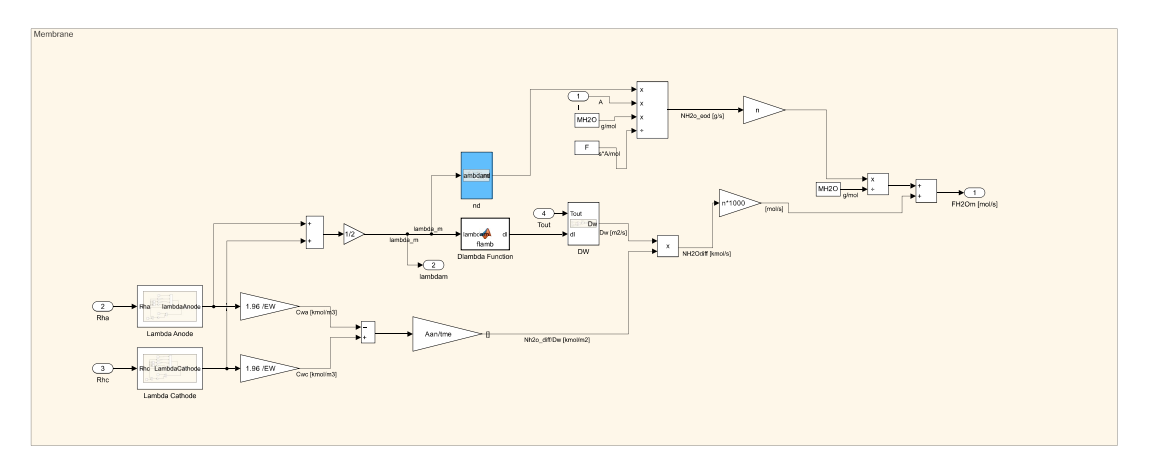


Figure 44: Membrane scheme and blocks

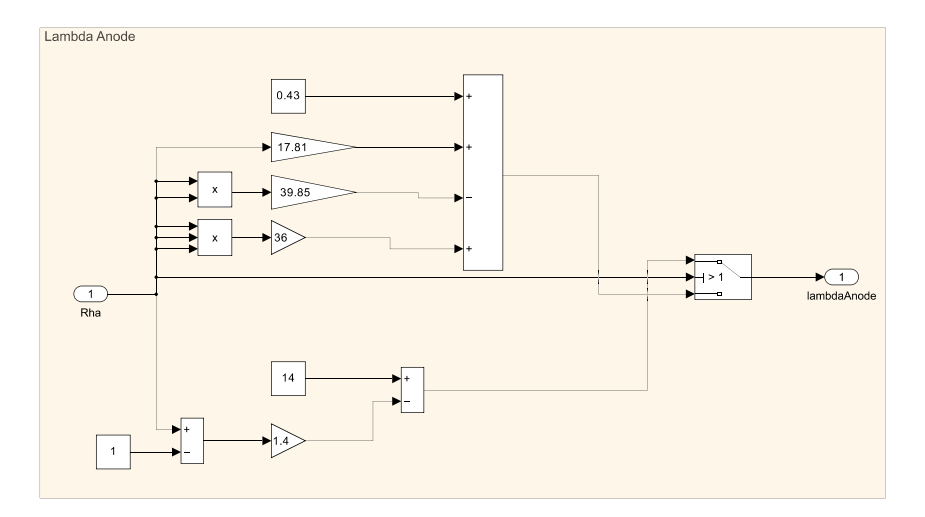


Figure 45: Water content at the anode

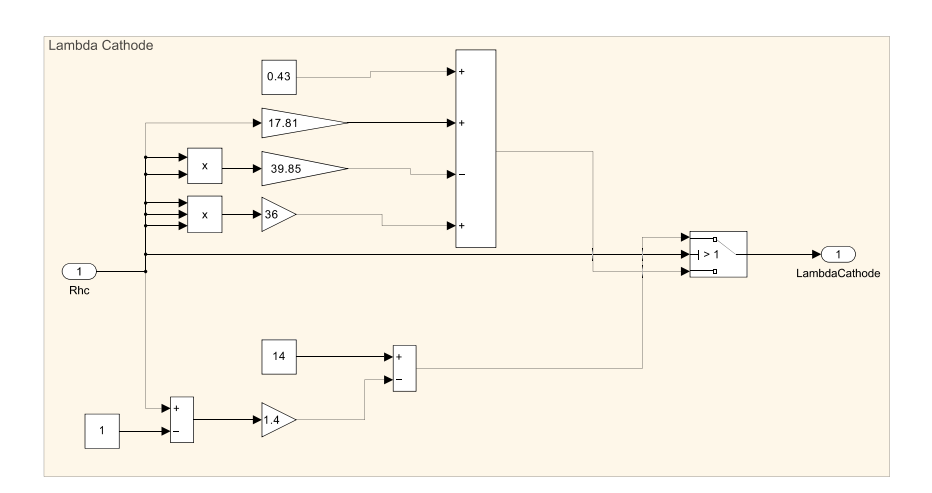


Figure 46: Water content at the cathode

page 72 Master Thesis

8.4 Voltage

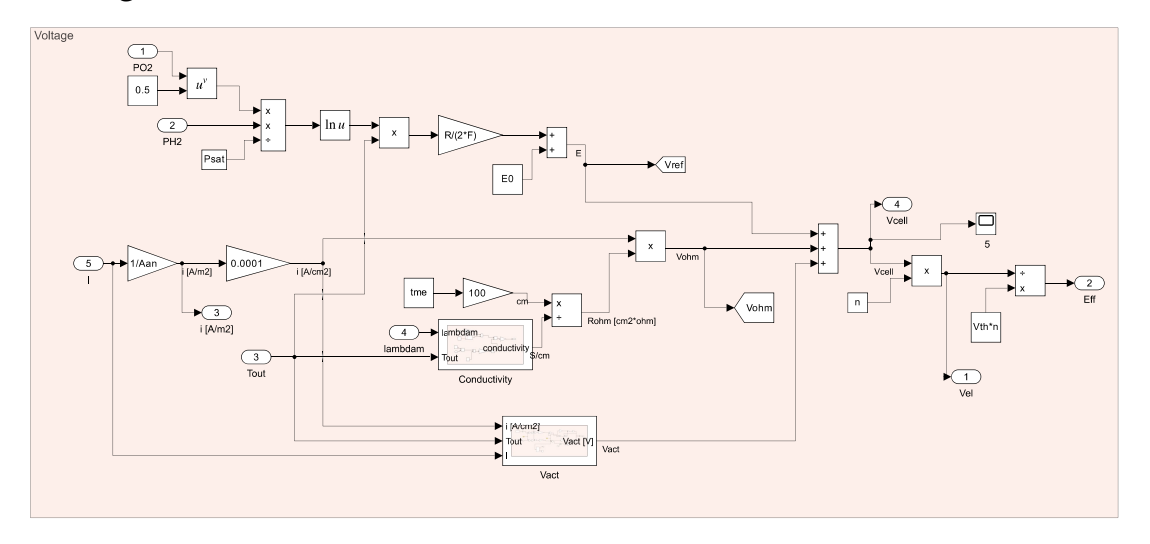


Figure 47: Voltage scheme and blocks

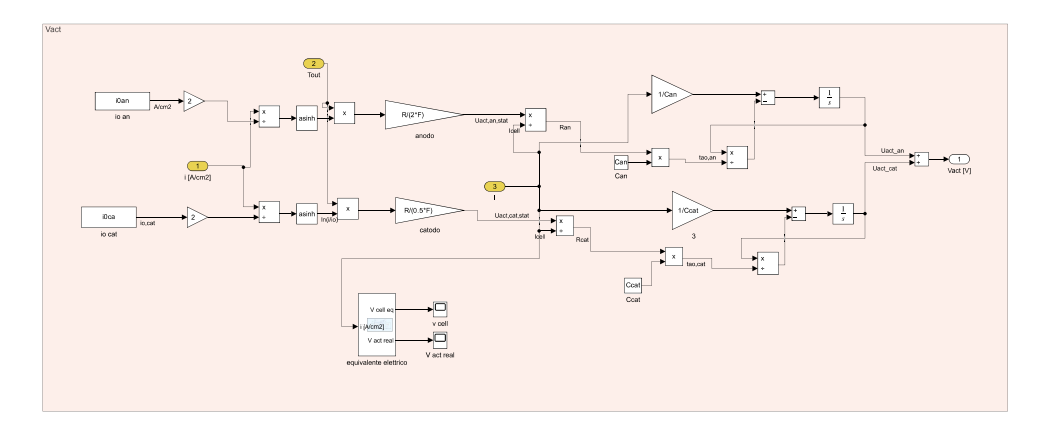


Figure 48: Activation overvoltage scheme and blocks

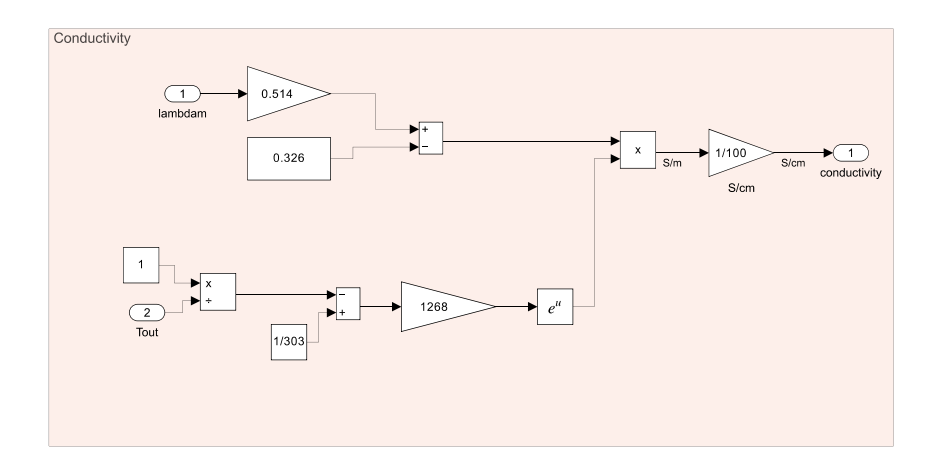


Figure 49: Conductivity calculation blocks

8.5 Thermal Block

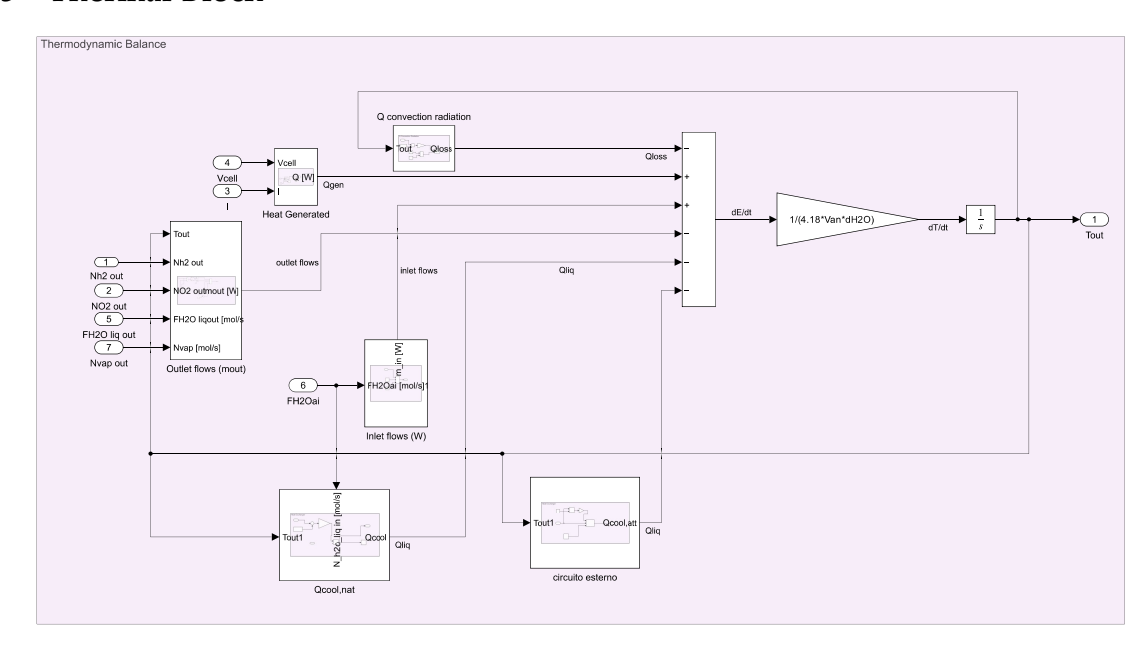


Figure 50: Thermodynamic balance scheme and blocks

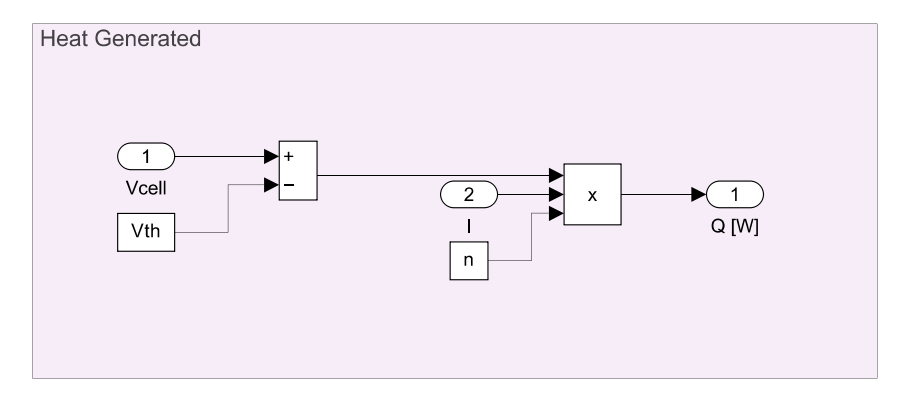


Figure 51: Heat generated scheme and blocks

page 74 Master Thesis

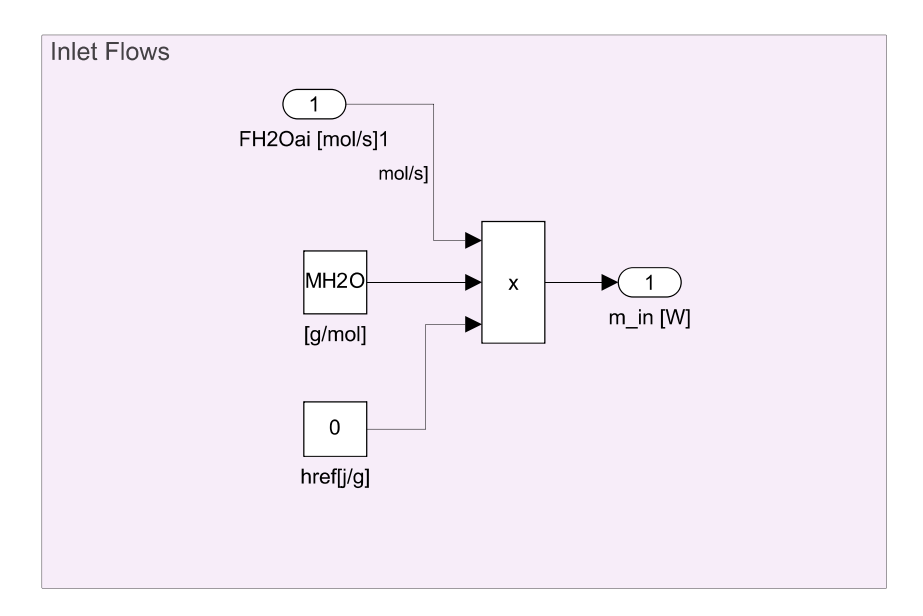


Figure 52: Inlet energy flows scheme

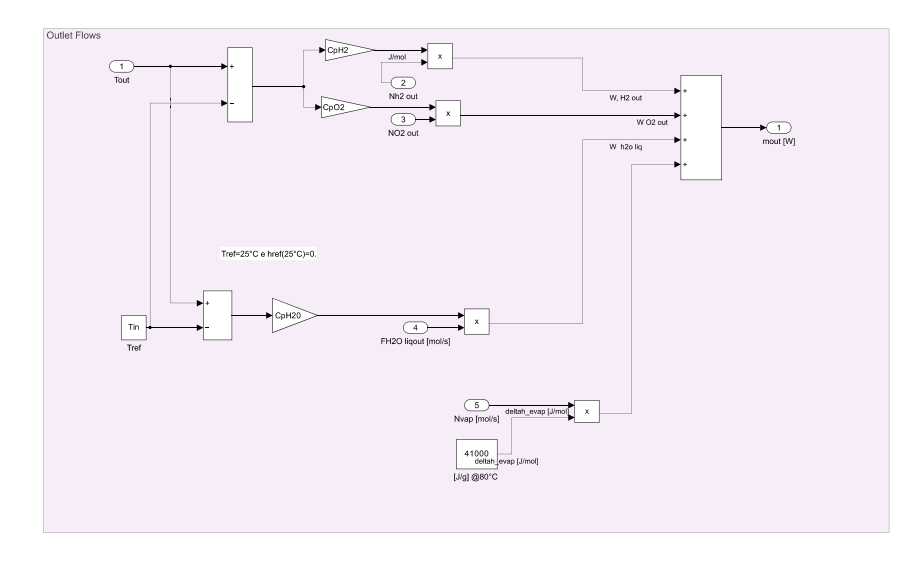


Figure 53: Outlet energy flows scheme

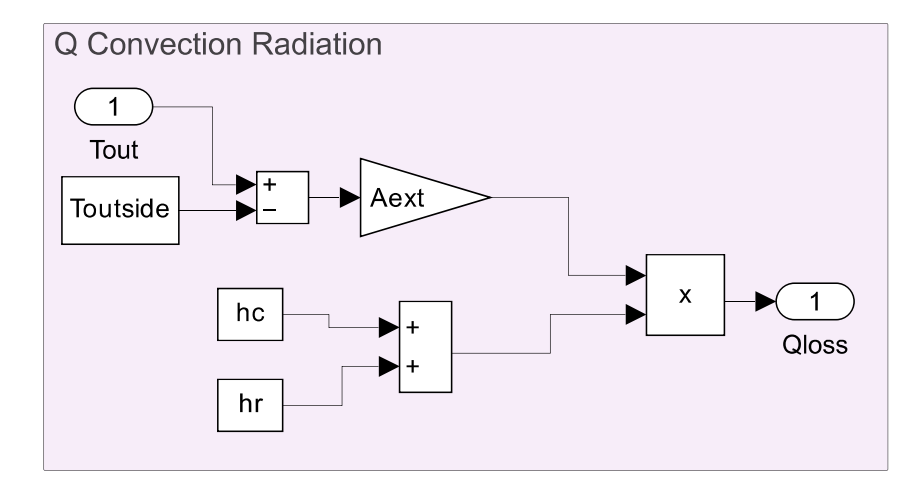


Figure 54: Convection and Radiation losses scheme and blocks

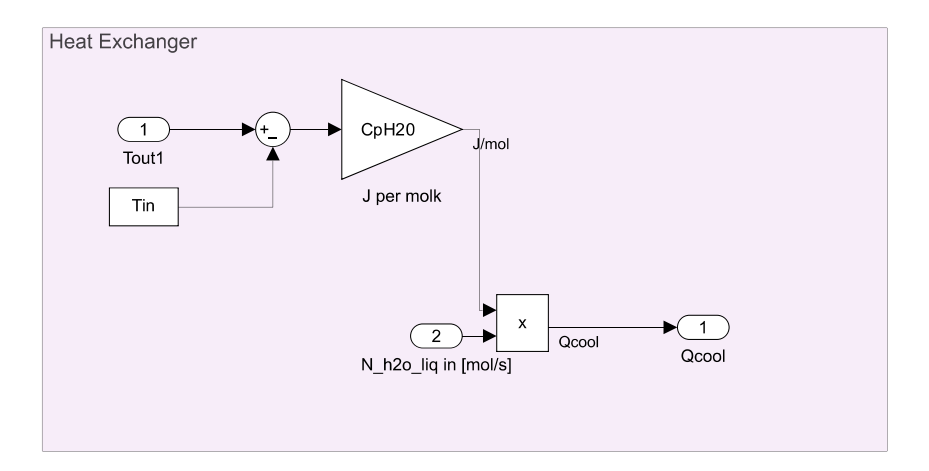


Figure 55: Passive cooling effect scheme

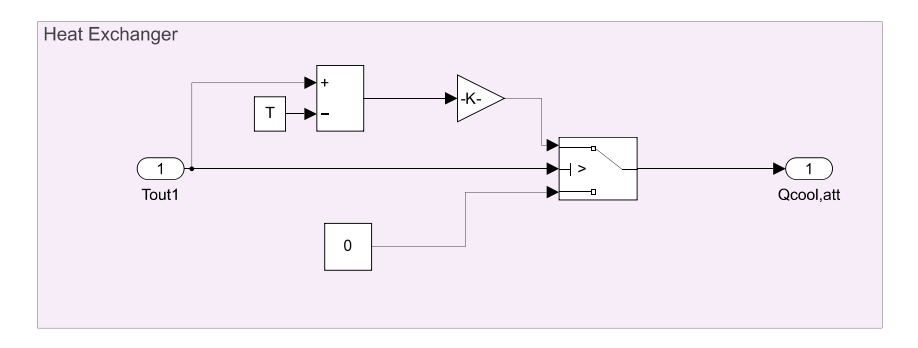


Figure 56: Additional active cooling effect scheme

BIBLIOGRAPHY page 77

Bibliography

[1] S. M. Alfredo Rivera and E. Rutkowski, "Global greenhouse gas emissions: 1990-2022 and preliminary 2023 estimates," *Rhodium group*.

- [2] E. Marro, "36 aziende producono la metà dell'inquinamento mondiale: il rapporto carbon majors," ilsole24ore, 2025.
- [3] "Europa: emissioni gas serra in calo ma non bisogna fermarsi," Ecquologia, 2025.
- [4] U. N. climate change, "The paris agreement," 2015.
- [5] N. A. Fae Jencks, "Climate trace begins monthly data releases with new greenhouse gas data showing january 2025 emissions worldwide," *Climate Trace*.
- [6] S. Bontempi, "I mondo è sempre più inquinato: emissioni in aumento nella prima metà del 2025," *HDgreen*, 2025.
- [7] E. Voccia, "Emissioni di co2, europa e usa in testa, cina in calo grazie alle rinnovabili," *Rinnovabili*, 2025.
- [8] J. M. M. Arcos and D. M. F. Santos, "The hydrogen color spectrum: Techno-economic analysis of the available technologies for hydrogen production," *Gases*, vol. 3, no. 1, pp. 25–46, 2023.
- [9] S. Chai, G. Zhang, G. li, and Y. Zhang, "Industrial hydrogen production technology and development status in china: a review," *Clean Technologies and Environmental Policy*, vol. 23, pp. 1–16, 09 2021.
- [10] N. Ghasem, "A review of the cfd modeling of hydrogen production in catalytic steam reforming reactors," *International Journal of Molecular Sciences*, vol. 23, no. 24, 2022.
- [11] K. W. M. Ouellette, "Carbon capture, utilization, and storage: An entrepreneurial approach to reducing ghg emissions," *MEI*, *Ideas for a more prosperous society*.
- [12] S. G. Michael Kobina Kane, "Green hydrogen: A key investment for the energy transition,"
- [13] G. Chandler, "Low-emission hydrogen from natural gas,"
- [14] P. R. Hannah Ritchie, "Electricity mix,"
- [15] C. of the desert, "Hydrogen fuel cell engines and related technologies," 2001.
- [16] B. Yodwong, D. Guilbert, M. Phattanasak, W. Kaewmanee, M. Hinaje, and G. Vitale, "Ac-dc converters for electrolyzer applications: State of the art and future challenges," *Electronics*, vol. 9, no. 6, 2020.
- [17] P. Farràs, P. Strasser, and A. J. Cowan, "Water electrolysis: Direct from the sea or not to be?," *Joule*, vol. 5, no. 8, pp. 1921–1923, 2021.
- [18] S. G. Simoes, J. Catarino, A. Picado, T. F. Lopes, S. di Berardino, F. Amorim, F. Gírio,

page 78 Master Thesis

C. Rangel, and T. Ponce de Leão, "Water availability and water usage solutions for electrolysis in hydrogen production," *Journal of Cleaner Production*, vol. 315, 2021.

- [19] H. Becker, J. Murawski, D. V. Shinde, I. E. L. Stephens, G. Hinds, and G. Smith, "Impact of impurities on water electrolysis: a review," *Sustainable Energy Fuels*, vol. 7, pp. 1565–1603, 2023.
- [20] G. Athanasaki, A. Jayakumar, and A. Kannan, "Gas diffusion layers for pem fuel cells: Materials, properties and manufacturing a review," *International Journal of Hydrogen Energy*, vol. 48, no. 6, pp. 2294–2313, 2023.
- [21] F. Zhang, P. Zhao, M. Niu, and J. Maddy, "The survey of key technologies in hydrogen energy storage," *International Journal of Hydrogen Energy*, vol. 41, no. 33, pp. 14535–14552, 2016.
- [22] S. Shiva Kumar and H. Lim, "An overview of water electrolysis technologies for green hydrogen production," *Energy Reports*, vol. 8, pp. 13793–13813, 2022.
- [23] Q. Feng, X. Yuan, G. Liu, B. Wei, Z. Zhang, H. Li, and H. Wang, "A review of proton exchange membrane water electrolysis on degradation mechanisms and mitigation strategies," *Journal of Power Sources*, vol. 366, 2017.
- [24] A. Benmehel, S. Chabab, A. L. Do Nascimento Rocha, M. Chepy, and T. Kousksou, "Pem water electrolyzer modeling: Issues and reflections," *Energy Conversion and Management: X*, vol. 24, p. 100738, 2024.
- [25] T. T. Konttinen, "Digital model of pem electrolysis for hydrogen and waste heat production with heat management," *Master's thesis, University of Oulu*, 2025.
- [26] S. Asiaban, D. Bozalakov, and L. Vandevelde, "Development of a dynamic mathematical model of pem electrolyser for integration into large-scale power systems," *Energy Conversion and Management: X*, vol. 23, p. 100610, 2024.
- [27] H. Marefatjouikilevaee, F. Auger, and J.-C. Olivier, "Static and dynamic electrical models of proton exchange membrane electrolysers: A comprehensive review," *Energies*, vol. 16, no. 18, 2023.
- [28] Wikipedia contributors, "Supercapacitor Wikipedia, the free encyclopedia." https://en.wikipedia.org/w/index.php?title=Supercapacitor&oldid=1311242602, 2025. [Online; accessed 20-September-2025].
- [29] R. Omrani and B. Shabani, "Hydrogen crossover in proton exchange membrane electroly-sers: The effect of current density, pressure, temperature, and compression," *Electrochimica Acta*, vol. 377, p. 138085, 2021.
- [30] Y. Li, H. Li, W. Liu, and Q. Zhu, "Optimization of membrane thickness for proton exchange membrane electrolyzer considering hydrogen production efficiency and hydrogen permeation phenomenon," *Applied Energy*, vol. 355, p. 122233, 2024.
- [31] M. Schalenbach, M. Carmo, D. L. Fritz, J. Mergel, and D. Stolten, "Pressurized pem water electrolysis: Efficiency and gas crossover," *International Journal of Hydrogen Energy*, vol. 38,

BIBLIOGRAPHY page 79

no. 35, pp. 14921–14933, 2013.

LIST OF FIGURES page 81

List of Figures

1	Sectors contributions to GHG emissions in 2022 [1]	. 7
2	GHG emissions trends during the years [5]	. 8
3	General scheme of black H2 production through coal gasification [9]	. 9
4	Steam methane reforming for grey H2 production [10]	. 10
5	CCUS scheme principle [11]	. 10
6	Green H2 production scheme [12]	. 11
7	Methane pyrolysis for hydrogen production [13]	. 11
8	Electricity production with sector contributions [14]	. 12
9	Renewable energy sources coupled to an electrolyser [16]	
10	Water sources and treatments [18]	. 16
11	General scheme of an Electrolyser [20]	. 17
12	Alkaline water electroyser cell scheme [22]	
13	Anion exchange membrane water electrolyser cell scheme [22]	
14	Solid oxide water electrolyser cell scheme [22]	
15	Proton Exchange Membrane (PEM) water electrolyser cell scheme [22]	. 21
16	Electrolyser general scheme blocks	
17	Double layer representation in an equivalent electrical circuit	
18	Stack temperature evolution	
19	Input current	
20	Voltage of a single cell in time	
21	Equivalent electrical circuit	
22	Voltage characteristic in the equivalent electrical circuit	
23	Pressures at the anode	
24	Pressures at the cathode	. 49
25	H2 production	. 50
26	Variable input current	. 51
27	Pressures at the electrodes	. 51
28	Voltage of a single cell in the electrical model	. 52
29	Voltage of a single cell in the chemical model	. 53
30	H2 production with a variable current input	. 54
31	Input power and current	. 55
32	Voltage of a single cell in time	
33	Pressures at the anode	
34	Pressures at the cathode	. 57
35	H2 production with a solar power input	
36	Sensitivity analysis for photovoltaic field	
37	Hydrogen and Oxygen crossover scheme [29]	
38	Hydrogen content on the anode side with respect to varying current density	
39	H2 percentage at the anode with different working Temperatures	
4 0	Anode scheme and blocks	
41	Hydrogen percentage in Oxygen scheme and blocks	. 69
42	Cathode scheme and blocks	
43	Oxygen crossover scheme and blocks	
44	Membrane scheme and blocks	
45	Water content at the anode	
46	Water content at the cathode	
47	Voltage scheme and blocks	. 72

page 82 Master Thesis

48	Activation overvoltage scheme and blocks	72
49	Conductivity calculation blocks	72
50	Thermodynamic balance scheme and blocks	73
51	Heat generated scheme and blocks	73
52	Inlet energy flows scheme	74
53	Outlet energy flows scheme	74
54	Convection and Radiation losses scheme and blocks	75
55	Passive cooling effect scheme	75
56	Additional active cooling effect scheme	75

LIST OF TABLES page 83

List of Tables

1	Combustion properties of Hydrogen, Methane, and Gasoline	13
2	Model parameters for the PEM electrolyzer	44
3	Resistance and capacitance values for anode and cathode sides	47
4	PV Data	54
5	Fit-in parameters	64

LIST OF TABLES page 85

Acknowledgments

Ai miei nonni, senza i quali non sarei qui a scrivere queste parole. A mia nonna Giovanna, seconda madre e modello di riferimento, che con grande pazienza, durante i primi anni di scuola, passava i pomeriggi a spiegarmi la matematica al telefono e ripassava con me le tabelline nel tragitto verso il mare. A mio nonno Pietro, per avermi insegnato tenacia e per aver sempre gioito dei miei traguardi (chiedendomi sempre il famoso libretto di voti non capendo che non si usa più cartaceo ormai).

Ai miei genitori, che mi hanno sempre supportata in qualsiasi mia decisione. A mia mamma, mio esempio di forza, la prima a credere sempre in me e a fare il tifo per i miei traguardi. A mio papà, che mi ha sempre spinta a ragionare di testa mia e mi ha insegnato un po' di leggerezza d'animo. Grazie per avermi permesso di inseguire i miei obbiettivi e i miei sogni, anche se questo mi ha portato lontano da casa.

A mio zio Sandro, per essere stato sempre al mio fianco.

Grazie a Claudio e Pasquale per essere stati la mia prima casa, lontano da casa. Grazie per avermi viziata con tutti i vostri dolci (mai a sufficienza), per i regali, per avermi ascoltato parlare di qualsiasi cosa e lamentare ogni giorno e per essermi sempre stati vicini quando ne avevo bisogno.

In particolare, Claudio, grazie per essere il fratello che non ho mai avuto. Sia a Palermo, a cinque minuti di distanza, sia a Torino, in cui ci separava soltanto una parete sottile quasi inesistente, sei stato il mio riferimento fisso. Grazie per i tè, per i ciobar, per i film e soprattutto per esserci sempre stato nonostante facessi sempre l'opposto di quello che mi dicevi di fare, aspettandomi lì pronto con un "te lo avevo detto" come rimprovero.

Grazie a Chiara e Federica, mie migliori amiche e consiglieri dai banchi di scuola. A Chiara, la mia metà, che mi ha visto ed è stata accanto in tutte le fasi della mia vita e che mi ha insegnato l'essenza della vera amicizia. A Federica, per la costante fiducia e per avermi insegnato a essere più buona con me stessa. Ad Alessio, Federico e Bianca per essere sempre stati una costante, anche quando le nostre strade si sono divise, per poi ritrovarsi ogni volta nella nostra bella isola.

Grazie a Pietro, per essere stato il mio compagno di viaggio a Barcellona e per avermi insegnato a prendere la vita con un po' più di leggerezza (e soprattutto, grazie per avermi insegnato un po' a ballare la salsa).

A Emanuele, per aver condiviso con me questa tesi, la scrivania, gioie e preoccupazioni. E a Giovanni, per essere stato un coinquilino perfetto, per le notti passate a parlare e a consultare i tarocchi.

A Lorenzo, per essere stato il tutor migliore che potessi avere e un carissimo amico, per aver portato gioia e allegria in ogni giornata trascorsa insieme. Thank you to the International room for the support with the thesis, for the coffees and the loving memories. Y gracias Milena y Claudio, comparto con vosotros algunos de los recuerdos más bellos de mi tiempo en España.

Grazie ai miei amici di Torino, sia ai nuovi fatti durante il percorso sia agli emigrati su come me. Soprattutto, grazie al gruppo degli Energetici per aver reso questi due anni a Torino gli anni più belli della mia vita. Ad Anita, per la tua amicizia e la tua dolcezza d'animo, sempre presente nonostante stessimo quasi sempre in città o paesi differenti. A Simona, per il supporto, per avermi mostrato forza e insegnato amor proprio. A Chiara per aver sempre portato allegria

page 86 Master Thesis

e semplicità, sempre care a me le cene e le lunghe serate che noi tre abbiamo passato insieme. A Raoul, per essere stato il mio primo vero amico e per la cura che hai sempre riservato nei miei confronti. A Gabri, per la tua costante presenza e per il tuo cuore d'oro. A Gianluca, per la tua gentilezza e per essere un così caro amico. A Marco, per i nostri interminabili podcast e sedute di analisi. A Luca, per le sere passate a studiare insieme tra liquore al caffè e appunti, per le cene in mensa e per i passaggi in bici. Per aver fatto sempre da orecchio silente e per aver illuminato tutte le giornate della sessione invernale.

Infinitamente grata di aver avuto voi nel mio percorso e di avervi nella mia vita.